ANALYSIS OF EX-VESSEL STEAM EXPLOSIONS FOR THE COMBUSTION ENGINEERING SYSTEM 80+ USING THE *GT3F*™ COMPUTER CODE

(Supplemental Report)

July 1994

64 pp

I. INTRODUCTION

This document supplements Reference [1], and includes calculated results for hypothetical ex-vessel steam explosions in the CE 80- reactors, using the computer code $GT3F^{TM}$ [2,3]. This supplement has been prepared in response to the review and comments, addressing [1], by Energy Research Inc. [4].

In Reference [1], fuel-water interactions resulting from the following three separate scenarios were simulated:

1. a central instrument tube rupture

2. an outer instrument tube rupture

3. multiple instrument tube rupture

The water pool in the above simulations was assumed to be at saturation initially, at 393 K [1]. The triggering, furthermore, was assumed to take place on the axis of symmetry of the molten fuel jet, 4.1 m above the bottom of the water pool.

Calculations, to be discussed below, were repeated for scenarios (1) and (2) above, in which, as recommended in [4]:

a) The water pool was assumed to be initially at 353 K (40K subcooled).

b) Triggering was assumed to occur at 4.5 m above the bottom of the water pool, which correctly corresponds to the mid-plane elevation of the submerged portion of the corbel support.

In addition, calculation results are also presented in this document which examine the effect of the assumed level of fuel fragmentation in the triggering spot, which sim-

ulates the triggering in the numerical calculations. on the predicted pressure histories during the propagation phase of the steam explosions.

II. CENTRAL INSTRUMENT TUBE FAILURE

II.1 Premixing

The system configuration, nodalization, time step, etc., were all identical to those described in Section 2.1 of [1], with the exception of item (a) above. The water was thus assumed to be at 353 K temperature initially.

The calculated results are depicted in the figures listed below, where, in this section and elsewhere in this document. wherever applicable, the figure numbers for the corresponding figures in [1] are also given in parentheses.

- Figure II.1 (corresponding to Figure 2.3 in [1]) Molten fuel volume fraction contours
- Figure II.2 (corresponding to Figure 2.4 in [1]) Void fraction (gas volume fraction) contours
- Figure II.3 (corresponding to Figure 2.5 in [1]) Pressure contours

II.2 Propagation

The system configuration, nodalization, time steps, etc., were identical to those described in Section 2.2 of [1]. However, as mentioned above, triggering was assumed to occur on the axis of symmetry of the molten fuel jet in the node (1.23), 4.5 m above the bottom of the water pool. The results are depicted in the figures listed below.

- Figure II.4 (corresponding to Figure 2.7 in [1]) Molten fuel volume fraction

- Figure II.5 (corresponding to Figure 2.8 in [1]) Void fraction (gas volume fraction) contours
- Figure II.6 (corresponding to Figure 2.9 in [1]) Pressure contours
- Figure II.7 (corresponding to Figure 2.10 in [1]) Pressure histories at various nodes
- Figure II.8 (corresponding to Figure 2.12 in [1]) Pressure impulse distributions

Pressure impulse distributions along the jet centerline (Figure II.8a) and along the corbel support surface (Figure II.8b, corresponding to Figure 2.12 in [1]) are both depicted. (Pressure impulses representing 20% fragmentation at triggering are also included in Figure II.8a which will be discussed in the forthcoming subsection.) These pressure impulses all represent 20 ms integration times. The calculated impulse values for the jet centerline (Figure II.8a) are realistic since, as noted in Figure II.7a, the pressures on the center line all decay to the base pressure within 20 ms. The pressure impulses for the corbel support surface depicted in Figure II.8b, however, do not represent the full impulses since, as noted in Figure II.7b, the pressures on the corbel support surface do not decrease to the base pressure within 20 ms after triggering.

The calculated maximum impulse on the centerline, as noted, is about 15 kPa.s, and takes place 4.8 m above the pool bottom. On the corbel support surface, the calculated pressure impulse decreases with height, from a maximum of about 6.8 kPa.s at the bottom elevation of the corbel support, to a minimum of about 5 kPa.s at the axial node (1,27) representing the water level height before the initiation of premix-

ing. The calculated pressure impulses for the corbel support surface, as mentioned above, do not represent the full impulse due to the short simulation time. They are, nevertheless, significantly lower than the 5th percentile impulse capacity for corbel support which is approximately 35 kPa.s [5]. Thus, it appears that the full impulse on the corbel support surface would also be considerably lower than the 5th percentile impulse capacity for the corbel support.

In Figure II.8a the calculated pressure impulses for an initially saturated water pool [1] are also depicted. The assumption of initially saturated water pool thus resulted in the underprediction of pressure impulses in the explosion zone.

II.3 Effect of Triggering Strength

All the simulation of the propagation phase in Reference [1], as well as everywhere in this document except for the case to be discussed in this subsection, were obtained by simulating the triggering assuming that, at the triggering time, 10% of the molten fuel in the node where triggering takes place (node (1,21) in [1] and node (1,23) everywhere in this document) underwent complete fragmentation in one time step.

Figure II.9 depicts pressure histories at various nodes during the propagation phase. These calculations were performed using all the parameters which were utilized in obtaining Figure II.7, except that triggering was simulated here by assuming 20% of the fuel in node (1,23) underwent complete fragmentation during one time step.

Comparing Figures II.7 and II.9, it can be noted that the pressure peaks in the triggered node (1,23) and the depicted adjacent nodes (1,21) and (1,25) are sensitive to triggering strength, as expected. The pressure peaks at nodes located further away from the triggering location, however, are only slightly affected. It thus appears that the important simulation results, and in particular the pressure histories on the

structural surfaces away from the triggering location, are relatively insensitive to the triggering strength.

Calculated pressure impulses resulting from 10% and 20% fragmentation at triggering are compared in Figure II.8a. As noted, the pressure impulses obtained with 20% fragmentation are slightly higher than those obtained with 10% fragmentation. The maximum impulse is increased from 15 kPA.s to about 16kPa.s in the explosion zone.

III. OUTER INSTRUMENT TUBE RUPTURE

III.1 Premixing

The system configuration, nodalization, time step, etc., were all identical to those described in Section 3.1 of [1], with the exception of item (a) described in Section I above. The water was thus assumed to be at 353 K temperature initially. The calculated results are depicted in the figures listed below.

- Figure III.1 (corresponding to Figure 3.3 in [1]) Molten fuel volume fraction contours
- Figure III.2 (corresponding to Figure 3.4 in [1]) Void fraction (gas volume fraction) contours
- Figure III.3 (corresponding to Figure 3.5 in [1]) Pressure contours

III.2 Propagation

The computation domain, depicted in Figure III.4, is a cylinder 300 cm in diameter, centered on the centerline of the molten fuel jet, as recommended in [4]. The simulated cylindrical domain thus replaces part of the solid structure, including the

corbel support, with liquid coolant. This was necessary for the 2-D calculations. Twenty-seven axial nodes, with $\Delta z = 20$ cm, and 50 radial nodes with $\Delta r = 3$ cm, were used. Other parameters were all similar to those described in Section 3.2 of [1], except for the location of triggering. As explained before, triggering was assumed to take place on the axis of symmetry of the molten fuel jet 4.5 m above the bottom of the water pool, in node (1,23).

The results are depicted in the figures listed below.

- Figure III.5 Molten fuel volume fraction contours
- Figure III.6 Void fraction (gas volume fraction) contours
- Figure III.7 Pressure contours
- Figure III.8 Pressure histories at various nodes
- Figure III.9 Pressure impulse distributions

Calculated pressure impulses on the corbel support surface, as noted, are in the 8.5 kPa.s to 13.0 kPa.s range, and are thus lower than those calculated in [1] by an order of magnitude. These pressure impulses represent 20 ms of integration time, and are realistic because, as can be seen in Figure III.8, within 20 ms after triggering the pressures decrease to the base value. Calculations using the nodalization scheme in [1] were highly conservative and overpredicted the pressure impulses on the corbel support surface due to the imposition of a rigid boundary around the 30 cm-diameter cylindrical computational domain. The calculated results depicted in Figure 3.9, on the other hand, are believed to underpredict the pressure impulses. A 3-D analysis

appears necessary for a more rigorous analysis. The aforementioned two 2-D solution results, nevertheless, can be assumed to bracket the 3-D calculation results.

REFERENCE

1. *Analysis of Ex-vessel Steam Explosions for the Combustion Engineering System 80+ using the GT3F^{TM} Computer Code*, Attachment to letter from S. I. Abdel-Khalik and S. M. Ghiaasiaan to M. Khatib-Rahbar (June 3, 1994).

2. W. M. Ren, S. M. Ghiaasiaan, and S. I. Abdel-Khalik, *GT3F: An Implicit Finite-Difference Computer Code for Transient Three-Dimensional Three-Phase Flow Part I: Governing Equations and Solution Scheme*, Numerical Heat Transfer, Part B: Fundamental, Vol. 25, pp. 1-20, 1994.

3. W. M. Ren, S. M. Ghiaasiaan, and S. I. Abdel-Khalik, *GT3F: An Implicit Finite-Difference Computer Code for Transient Three-Dimensional Three-Phase Flow Part II: Applications*, Numerical Heat Transfer, Part B: Fundamental, Vol. 25, pp. 21-38, 1994.

4. *CE System 80+ Ex-vessel Calculations Using GT3F^{TM} Computer Code*, Memo, dated June 13, 1994, from H. Esmaili to M. Khatib-Rahbar, Energy Research, Inc.

5. H. Esmaili and M. Khatib-Rahbar, *Analysis of Ex-vessel Steam Explosions for the Combustion Engineering System 80+*, ERI/NRC 94-201, Energy Research, Inc. March 1994.

Figure II.1 (Corresponding to Figure 2.3 in [1])
Central Instrument Tube Failure–Premixing
Fuel Volume Fraction
(Δr = 3.0 cm, Δz = 20.0 cm)

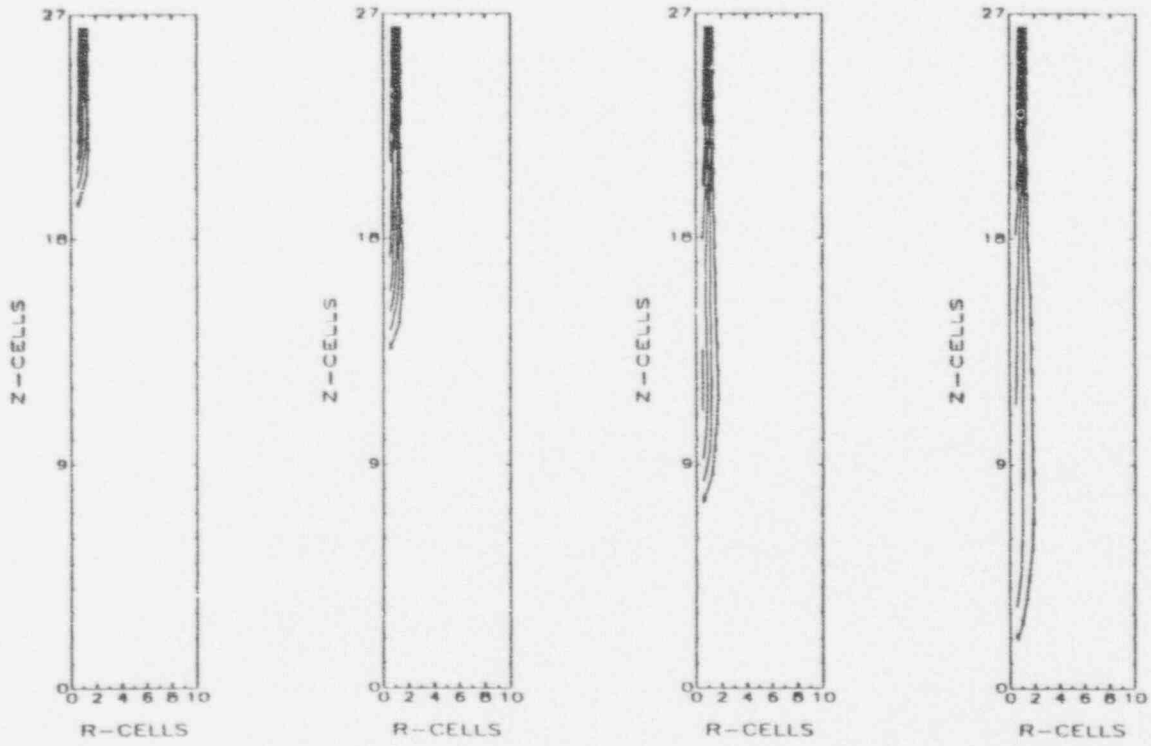

0.25 sec	0.50 sec	0.75 sec	1.00 sec
H=0.2402	H=0.2464	H=0.2471	H=0.2442
L=0.0000	L=0.0000	L=0.0000	L=0.0000

Figure II.2 (Corresponding to Figure 2.4 in [1])
Central Instrument Tube Failure–Premixing
Void Fraction
($\Delta r = 3.0$ cm, $\Delta z = 20.0$ cm)

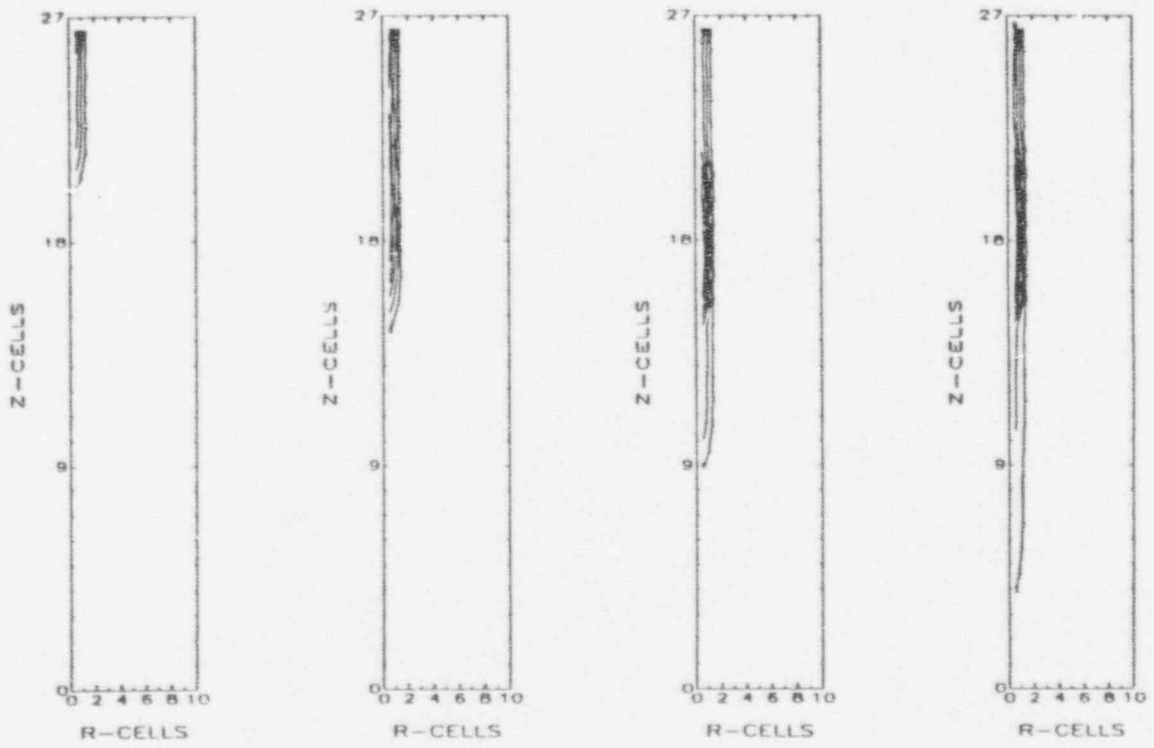

0.25 sec	0.50 sec	0.75 sec	1.00 sec
H=0.7062	H=0.5477	H=0.7382	H=0.7212
L=0.0001	L=0.0001	L=0.0001	L=0.0001

Figure II.3 (Corresponding to Figure 2.5 in [1])
Central Instrument Tube Failure–Premixing
Pressure (bar)
($\Delta r = 3.0$ cm, $\Delta z = 20.0$ cm)

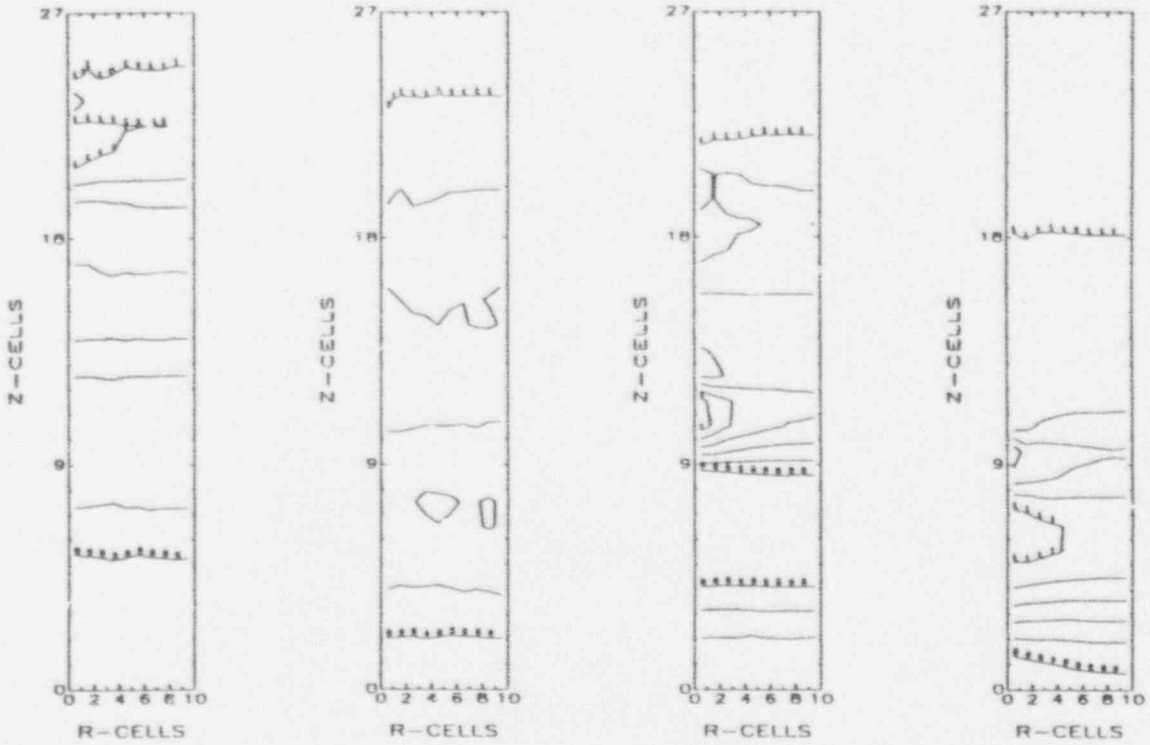

0.25 sec	0.50 sec	0.75 sec	1.00 sec
H=2.493	H=2.465	H=2.679	H=3.053
L=1.984	L=2.019	L=2.016	L=1.976

Figure II.4 (Corresponding to Figure 2.7 in [1])
Central Instrument Tube Failure–Propagation
Fuel Volume Fraction
(Δr = 3.0 cm, Δz = 20.0 cm)

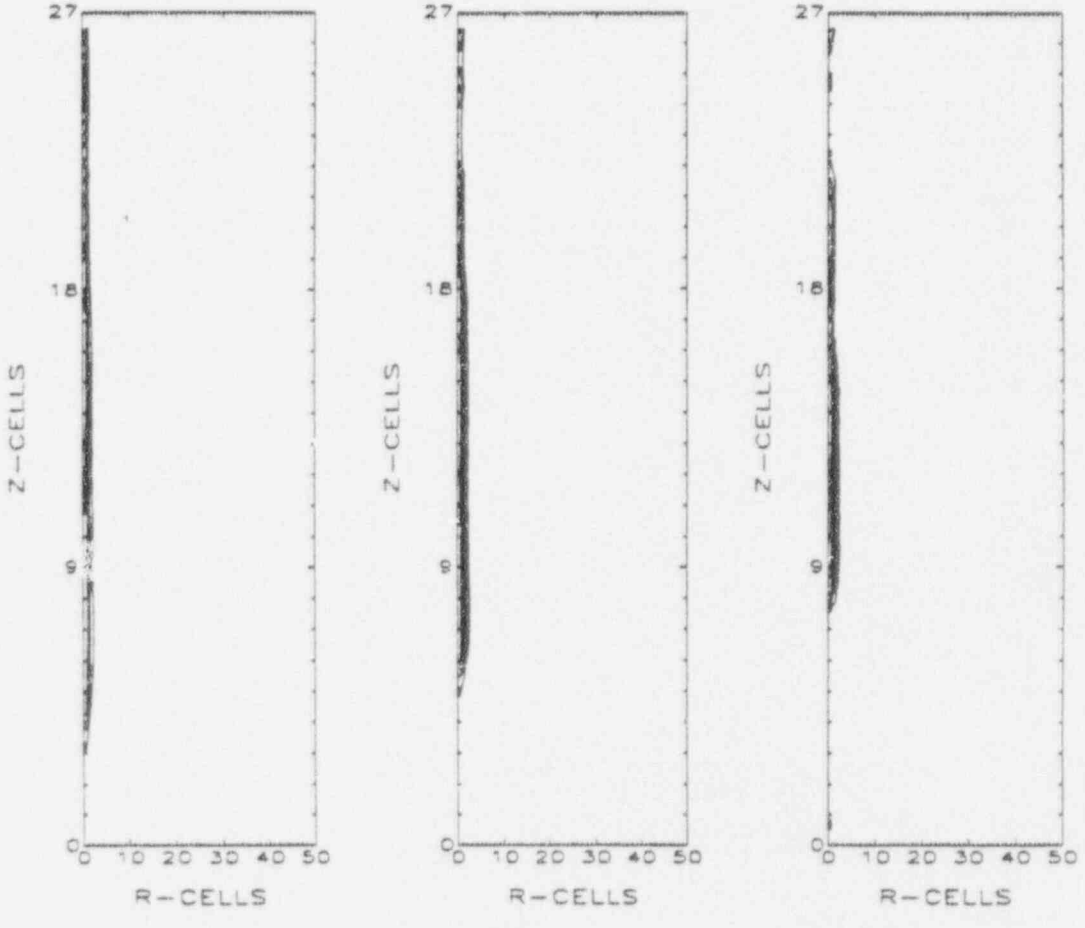

2.5 ms
H=0.2332
L=0.0000

5.0 ms
H=0.1322
L=0.0000

7.5 ms
H=0.1148
L=0.0000

Figure II.4 (contd)
Central Instrument Tube Failure–Propagation
Fuel Volume Fraction
(Δr = 3.0 cm, Δz = 20.0 cm)

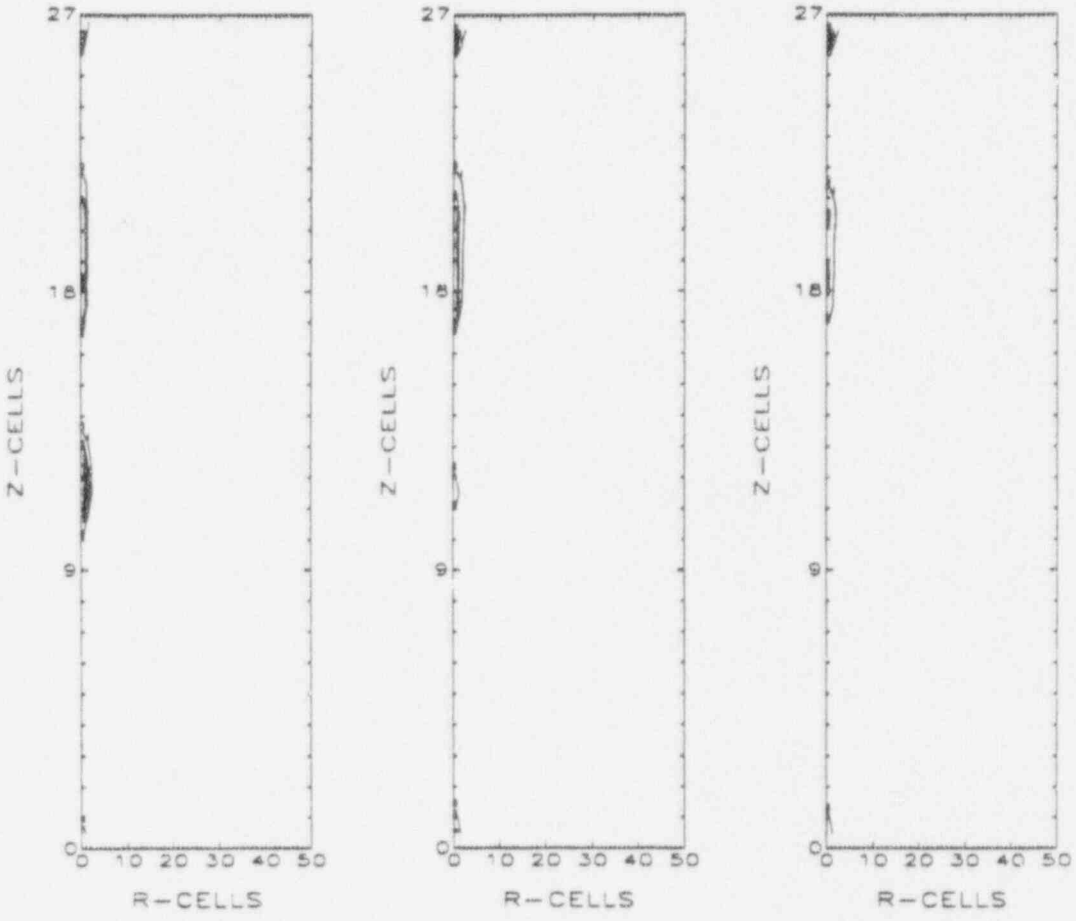

10.0 ms
H=0.0950
L=0.0000

12.5 ms
H=0.0515
L=0.0000

15.0 ms
H=0.0575
L=0.0000

Figure II.5 (Corresponding to Figure 2.8 in [1])
Central Instrument Tube Failure–Propagation
Void Fraction
($\Delta r = 3.0$ cm, $\Delta z = 20.0$ cm)

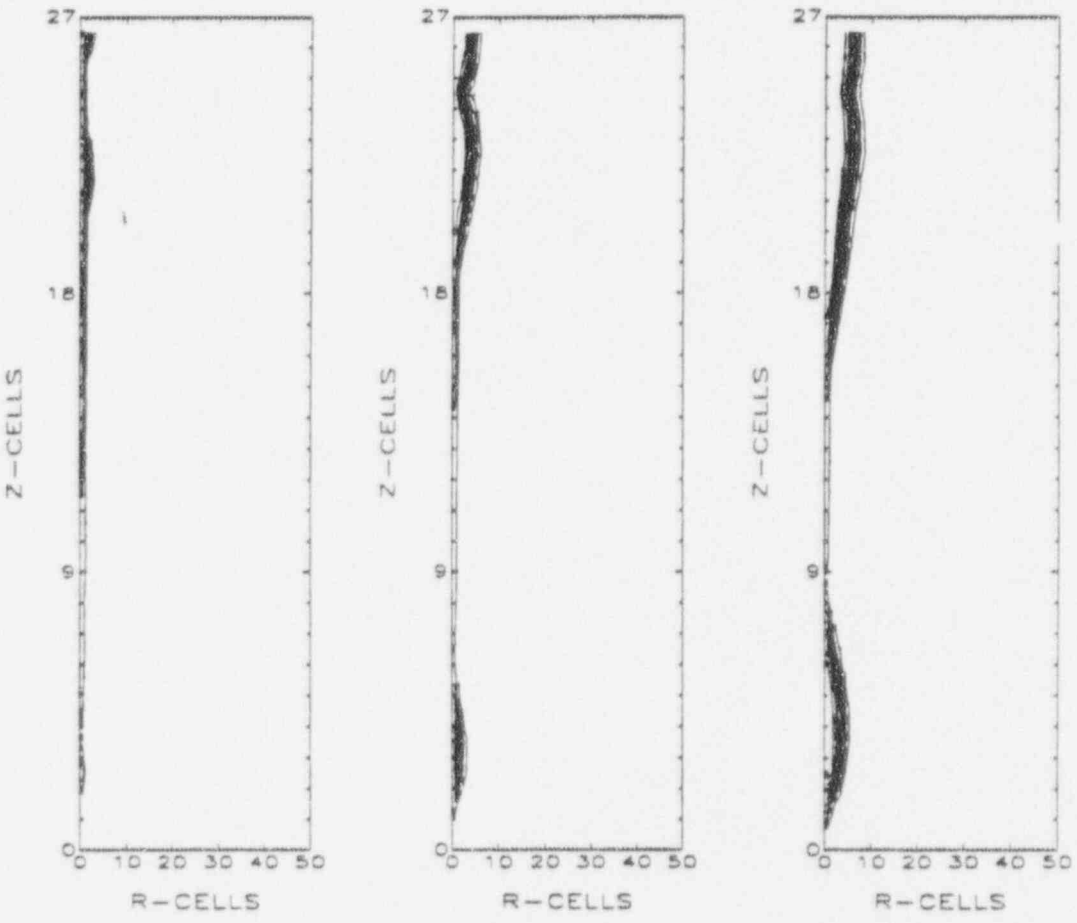

2.5 ms
H=0.8791
L=0.0000

5.0 ms
H=0.9812
L=0.0000

7.5 ms
H=0.9944
L=0.0000

Figure II.5 (contd)
Central Instrument Tube Failure–Propagation
Void Fraction
(Δr = 3.0 cm, Δz = 20.0 cm)

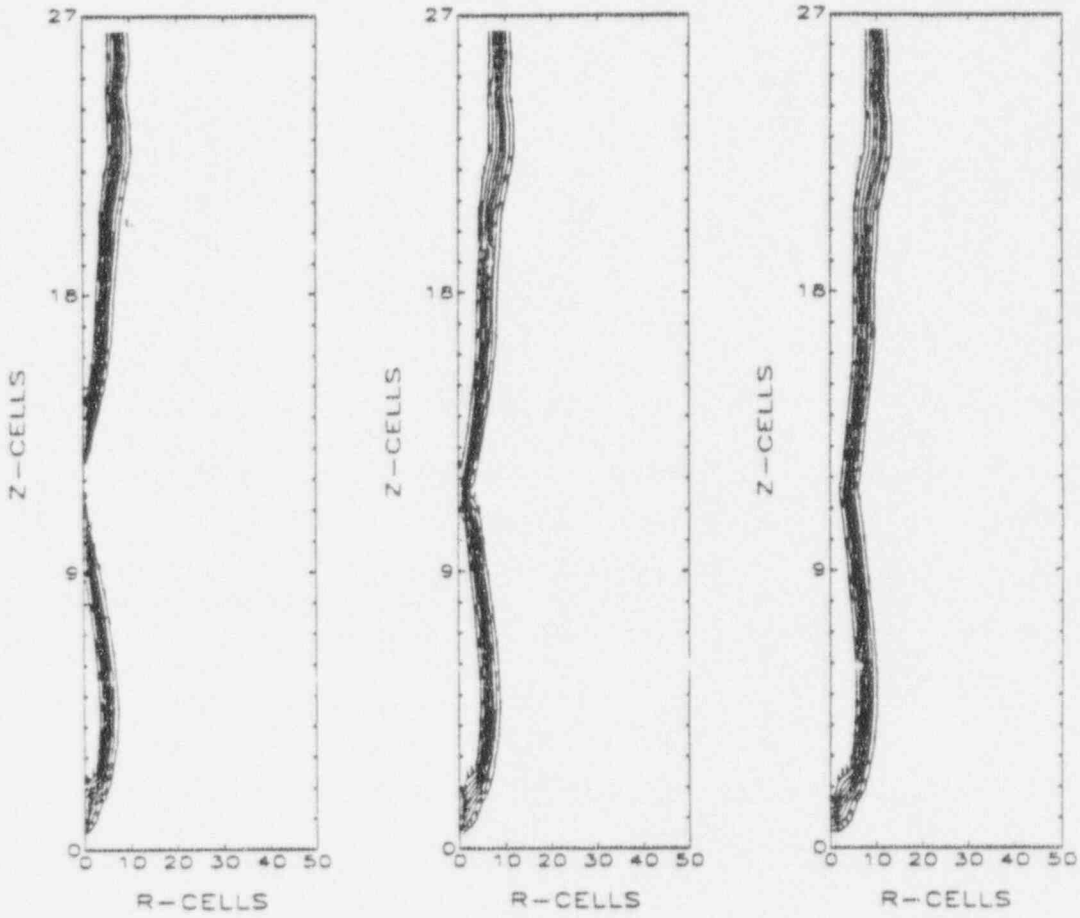

10.0 ms
H=0.9976
L=0.0000

12.5 ms
H=0.9991
L=0.0000

15.0 ms
H=0.9996
L=0.0000

Figure II.6 (Corresponding to Figure 2.9 in [1])
Central Instrument Tube Failure–Propagation
Pressure (bar)
(Δr = 3.0 cm, Δz = 20.0 cm)

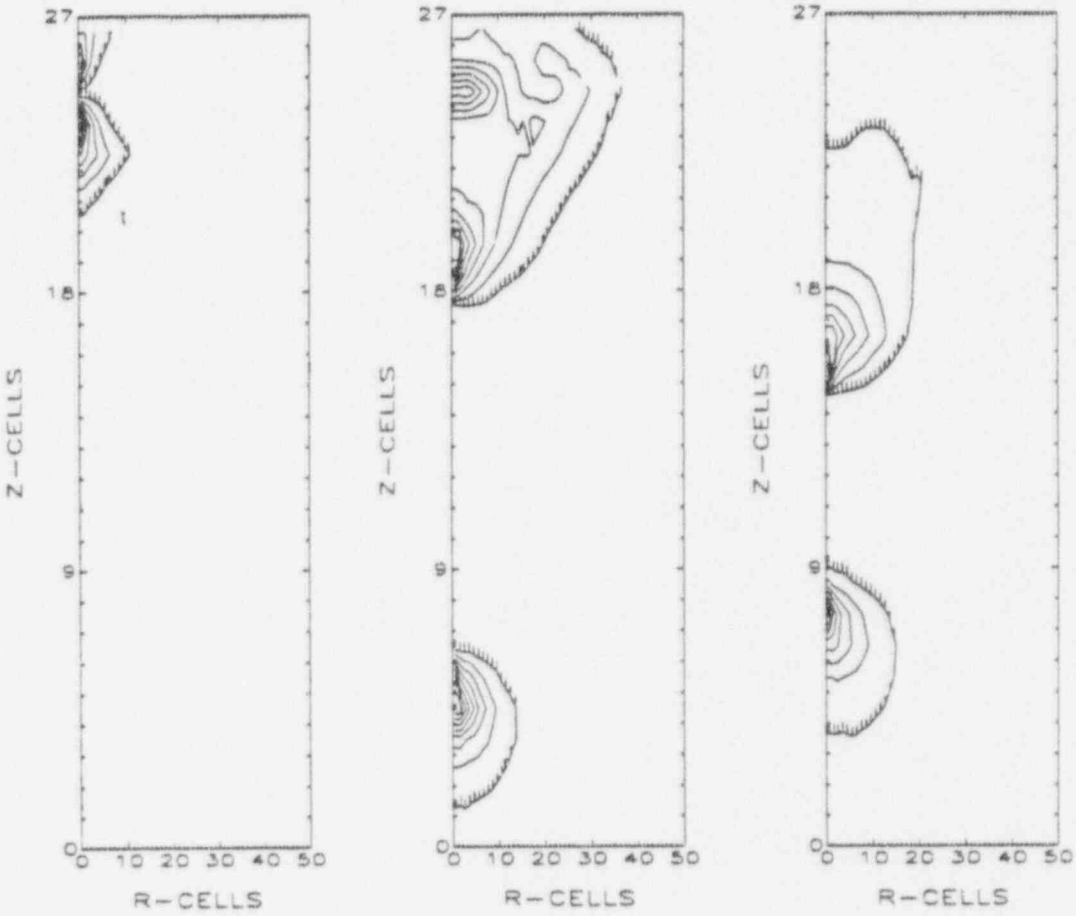

2.5 ms
H=66.86
L=1.895

5.0 ms
H=26.53
L=1.859

7.5 ms
H=44.88
L=1.897

Figure II.6 (contd)
Central Instrument Tube Failure–Propagation
Pressure (bar)
(Δr = 3.0 cm, Δz = 20.0 cm)

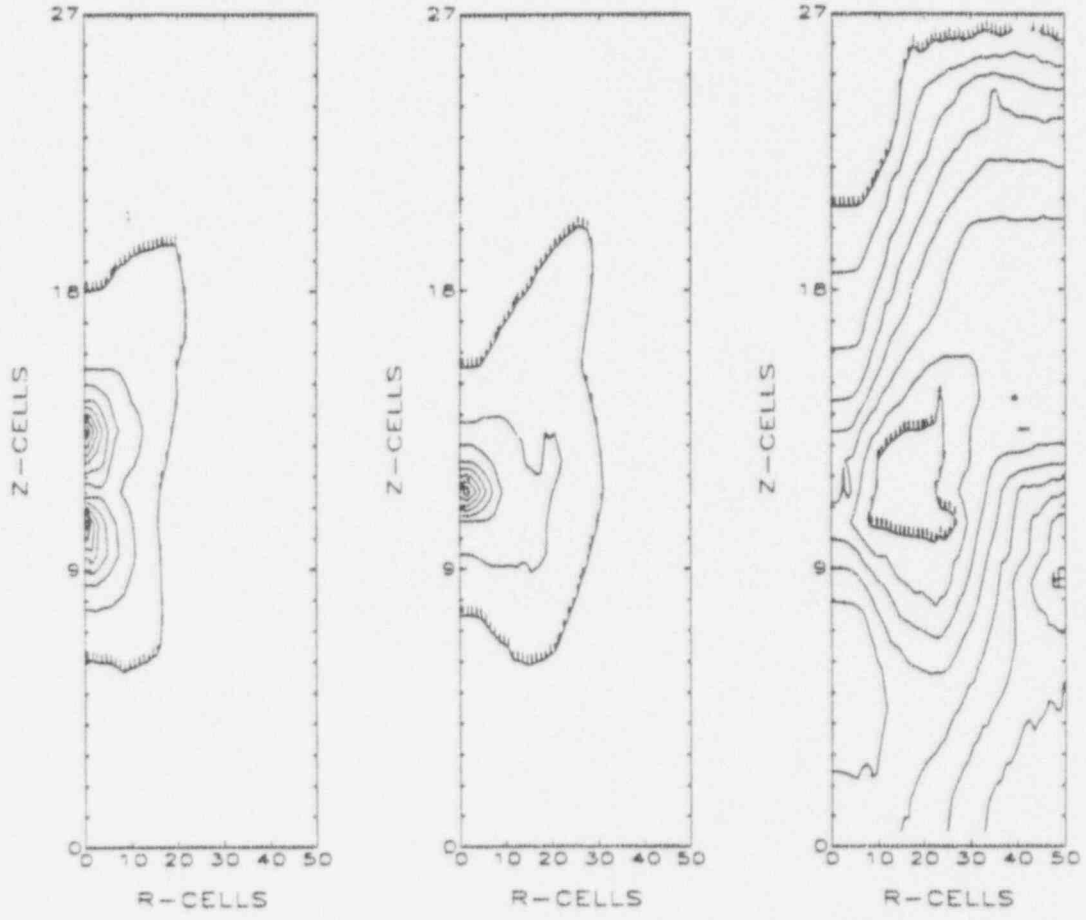

10.0 ms
H=44.23
L=2.162

12.5 ms
H=33.14
L=2.092

15.0 ms
H=7.161
L=1.853

Figure II.7 (Corresponding to Figure 2.10 in [1])
Central Instrument Tube Failure–Propagation
Pressure (bar)
(Δr = 3.0 cm, Δz = 20.0 cm, 10% Triggering)

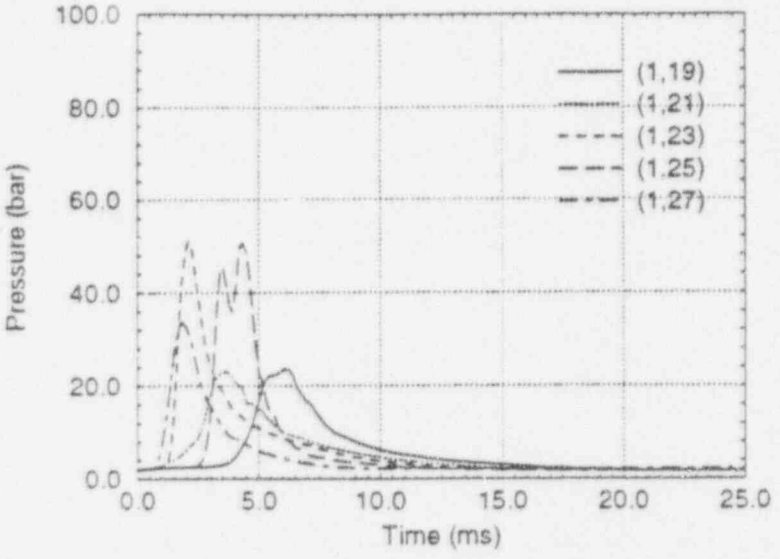

(a) Pressures along melt jet center line

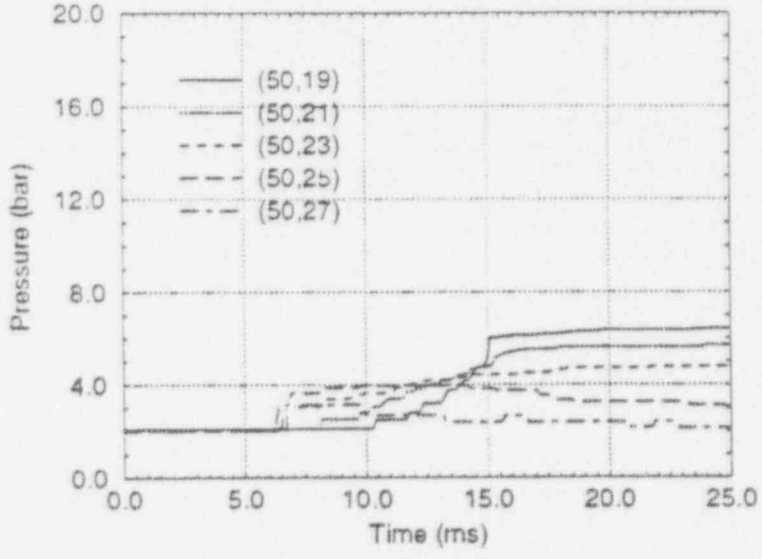

(b) Pressures along corbel support

Figure II.8
Central Instrument Tube Failure
Impulse ($KPa \cdot s$)
($\Delta r = 3.0$ cm, $\Delta z = 20.0$ cm)

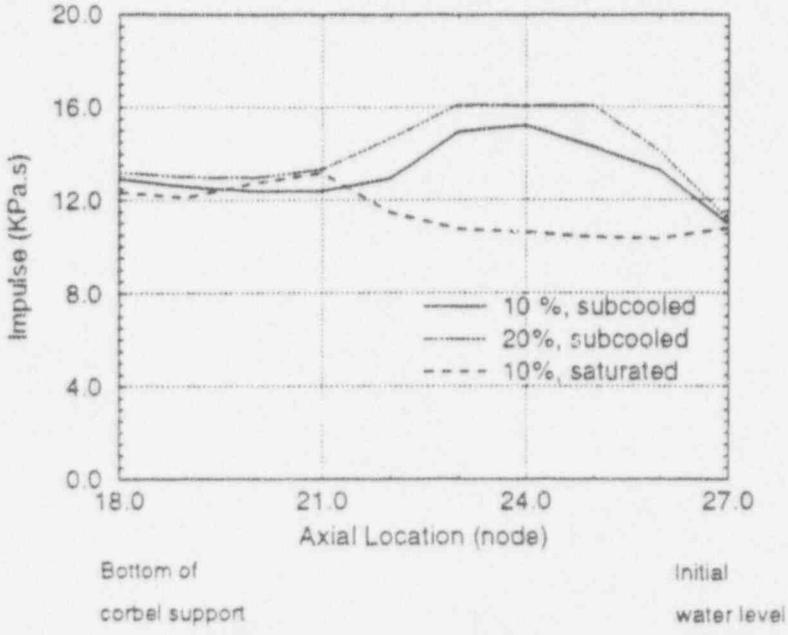

(a) Impulse Distribution Along Center Line

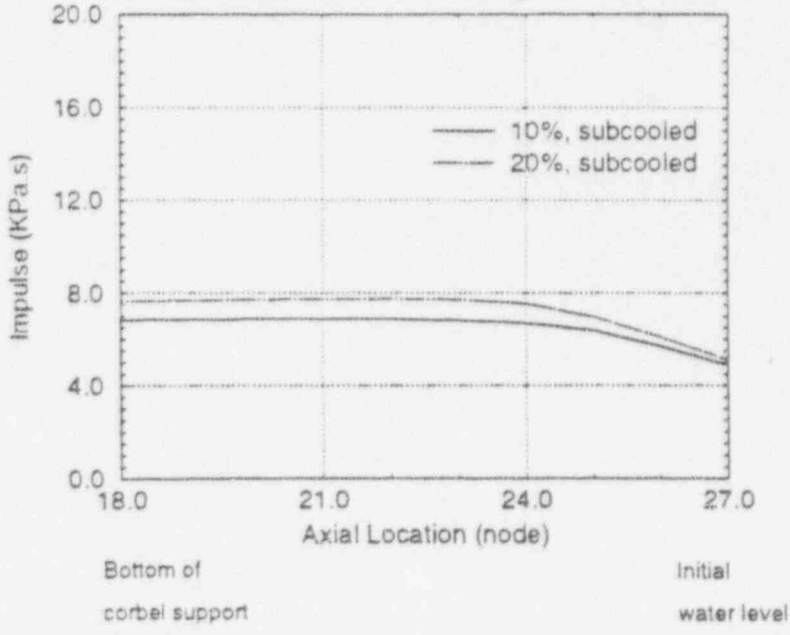

(b) Impulse Distribution Along Corbel Support

Figure II.9
Central Instrument Tube Failure–Propagation
Pressure (bar)
(Δr = 3.0 cm, Δz = 20.0 cm, 20% Triggering)

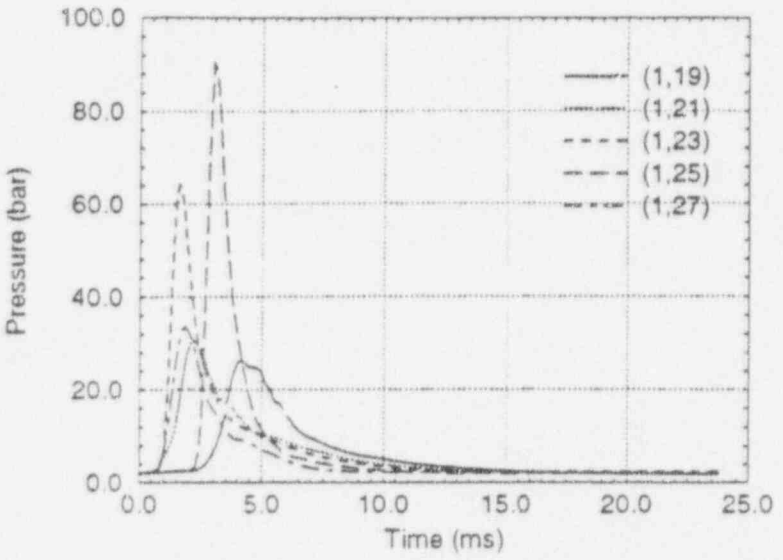

(a) Pressures along melt jet center line

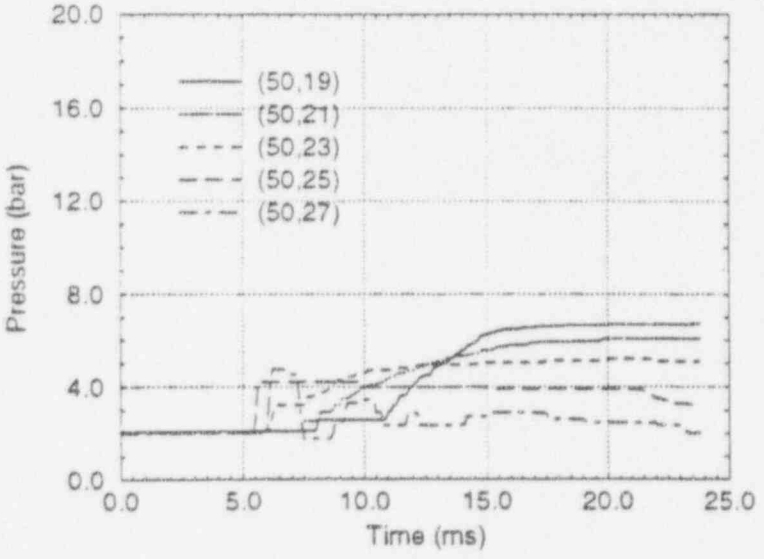

(b) Pressures along corbel support

Figure III.1 (Corresponding to Figure 3.3 in [1])
Outer Instrument Tube Failure–Premixing
Fuel Volume Fraction
($\Delta r = 3.0$ cm, $\Delta z = 20.0$ cm)

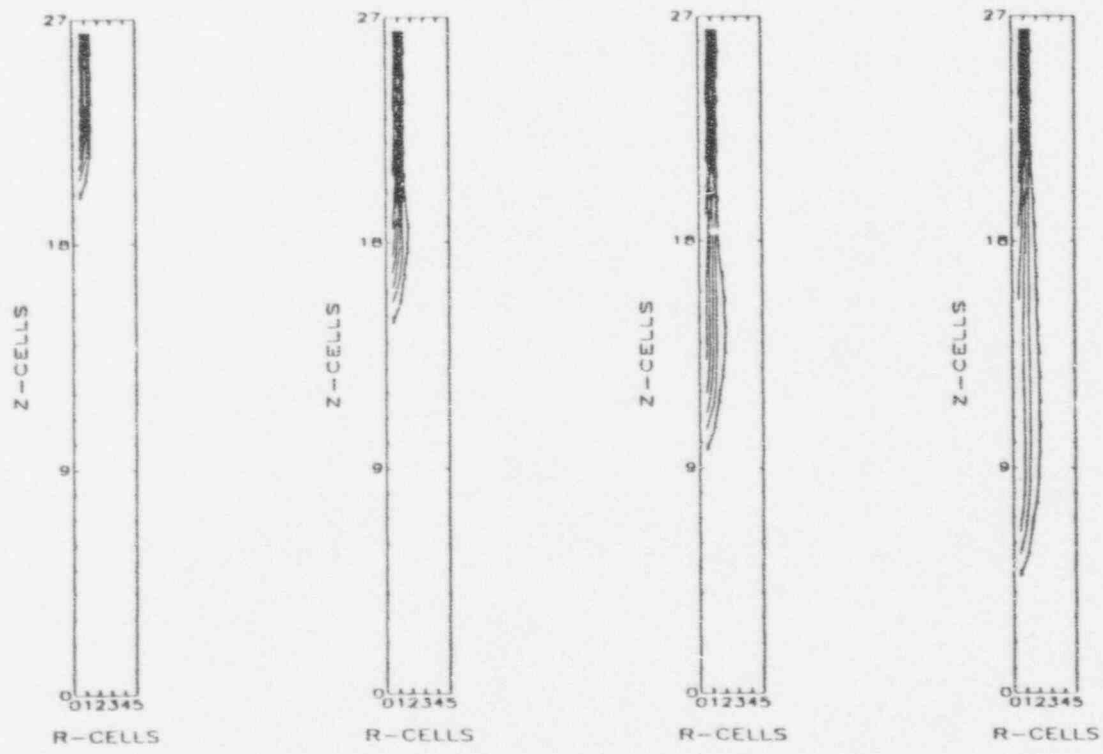

0.25 sec	0.50 sec	0.75 sec	1.00 sec
H=0.2333	H=0.2422	H=0.2447	H=0.2425
L=0.0000	L=0.0000	L=0.0000	L=0.0000

Figure III.2 (Corresponding to Figure 3.4 in [1])
Outer Instrument Tube Failure–Premixing
Void Fraction
($\Delta r = 3.0$ cm, $\Delta z = 20.0$ cm)

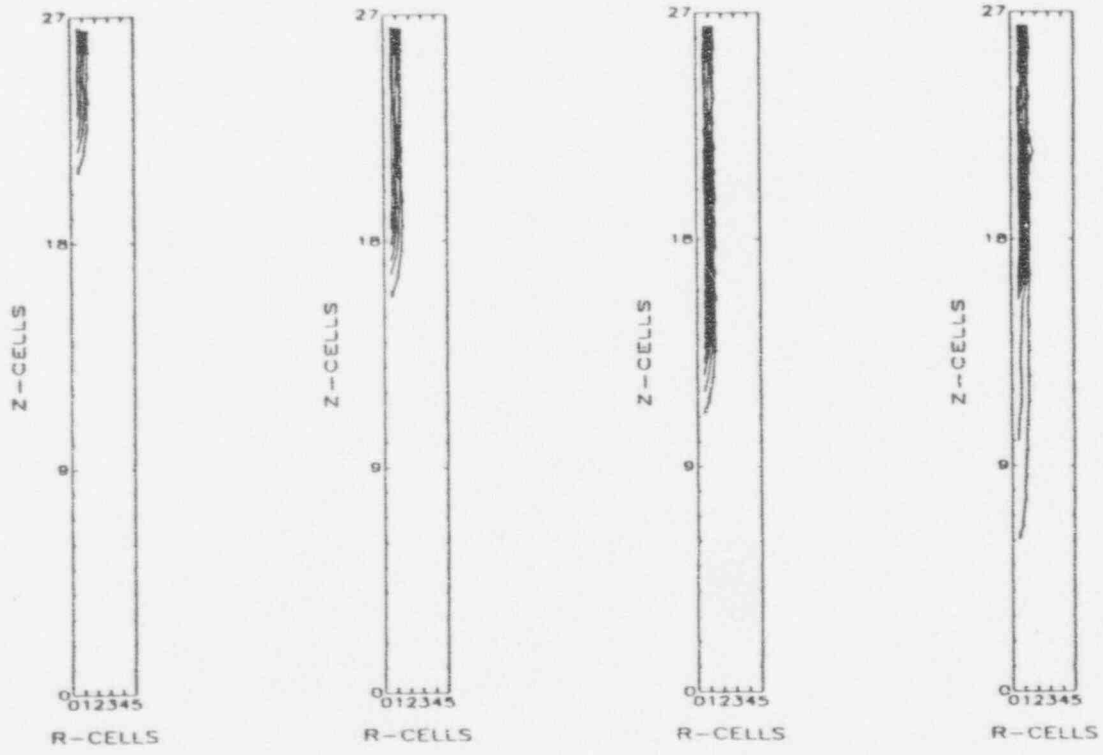

0.25 sec	0.50 sec	0.75 sec	1.00 sec
H=0.6894	H=0.5993	H=0.7001	H=0.6549
L=0.0001	L=0.0001	L=0.0001	L=0.0001

Figure III.3 (Corresponding to Figure 3.5 in [1])
Outer Instrument Tube Failure–Premixing
Pressure (bar)
(Δr = 3.0 cm, Δz = 20.0 cm)

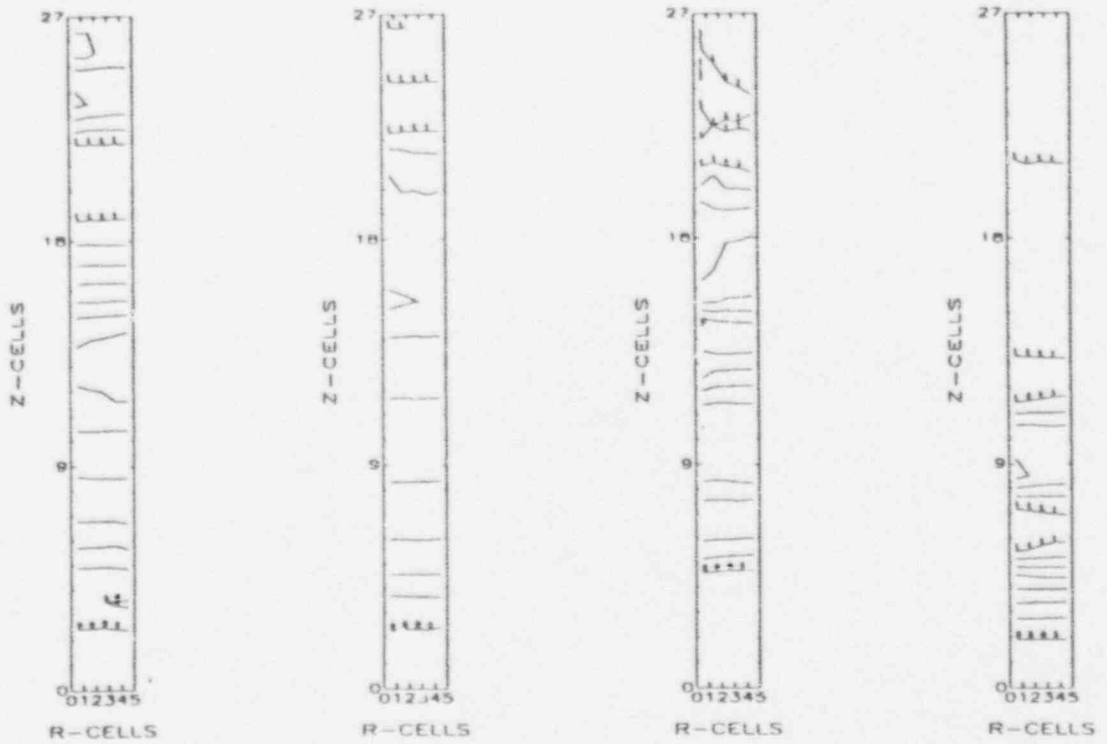

0.25 sec	0.50 sec	0.75 sec	1.00 sec
H=2.381	H=2.828	H=2.290	H=4.601
L=1.878	L=1.921	L=1.971	L=2.014

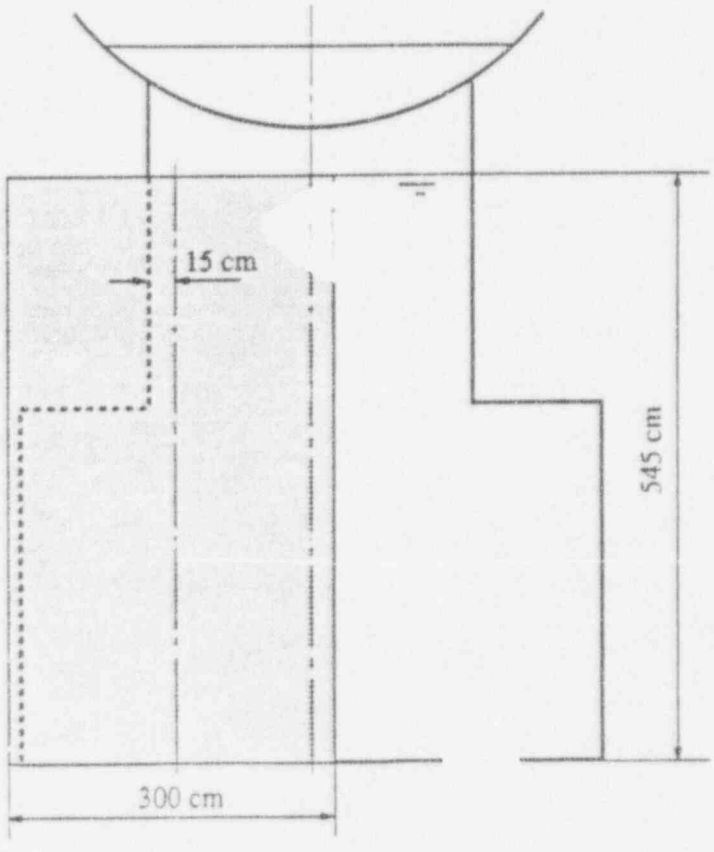

Figure III.4: Outer Instrument Tube Failure
(Shaded area represents computational domain for propagation calculation)

Figure III.5
Outer Instrument Tube Failure–Propagation
Fuel Volume Fraction
(Δr = 3.0 cm, Δz = 20.0 cm)

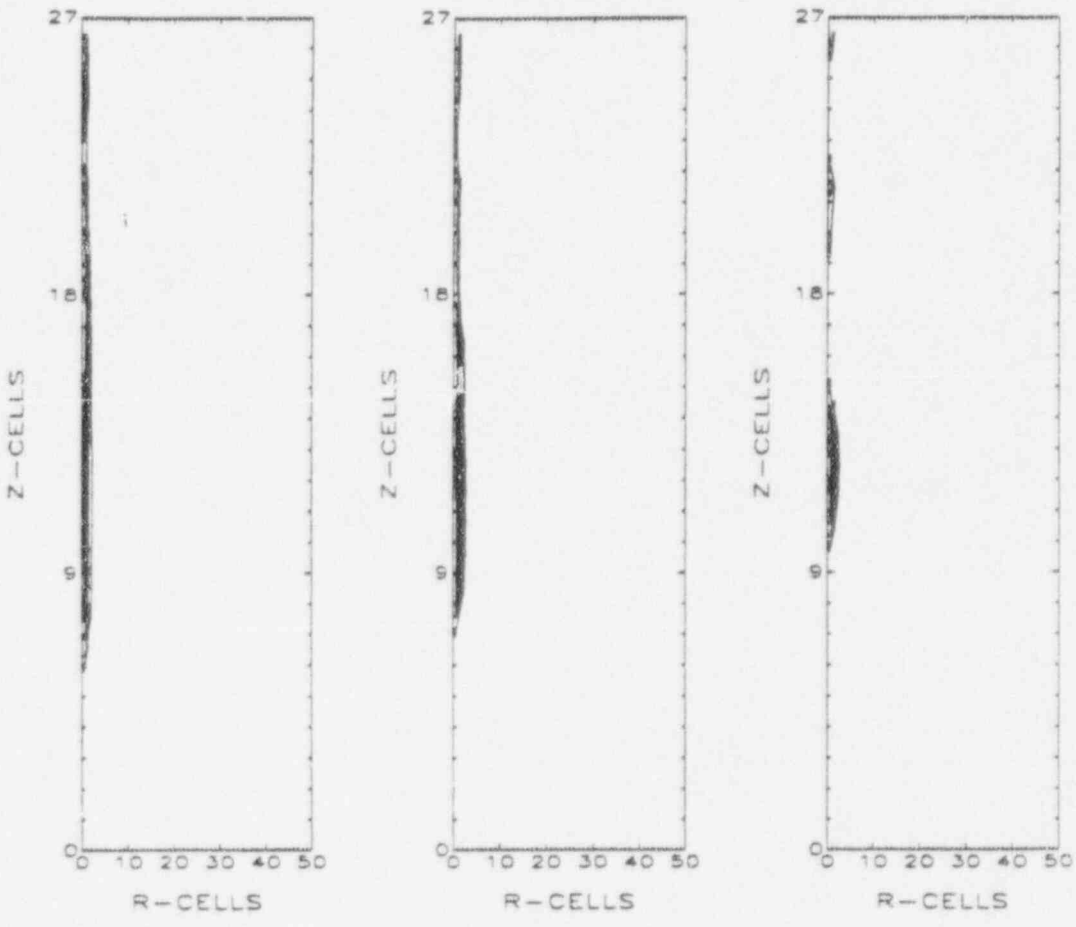

2.5 ms
H=0.2247
L=0.0001

5.0 ms
H=0.1080
L=0.0001

7.5 ms
H=0.1015
L=0.0001

Figure III.5 (contd)
Outer Instrument Tube Failure–Propagation
Fuel Volume Fraction
(Δr = 3.0 cm, Δz = 20.0 cm)

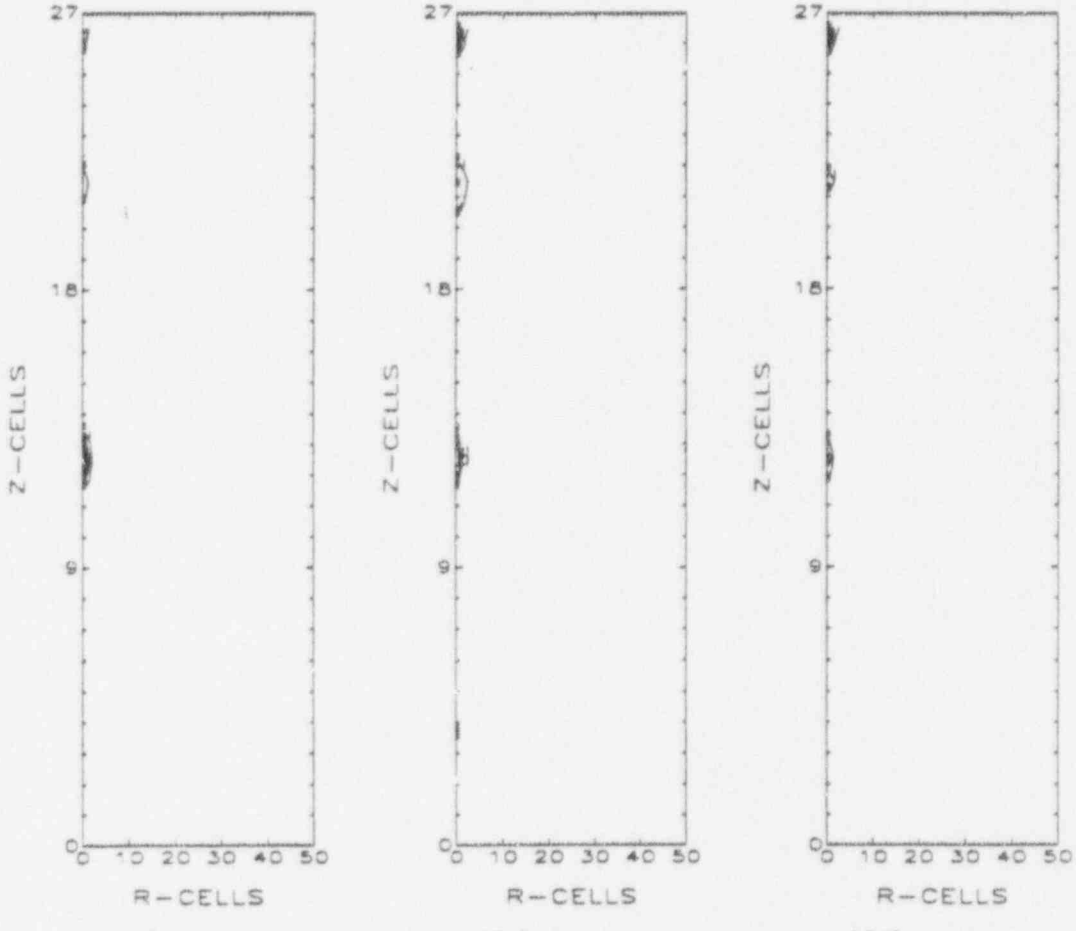

10.0 ms
H=0.0951
L=0.0001

12.5 ms
H=0.0419
L=0.0001

15.0 ms
H=0.0469
L=0.0001

Figure III.6
Outer Instrument Tube Failure–Propagation
Void Fraction
(Δr = 3.0 cm, Δz = 20.0 cm)

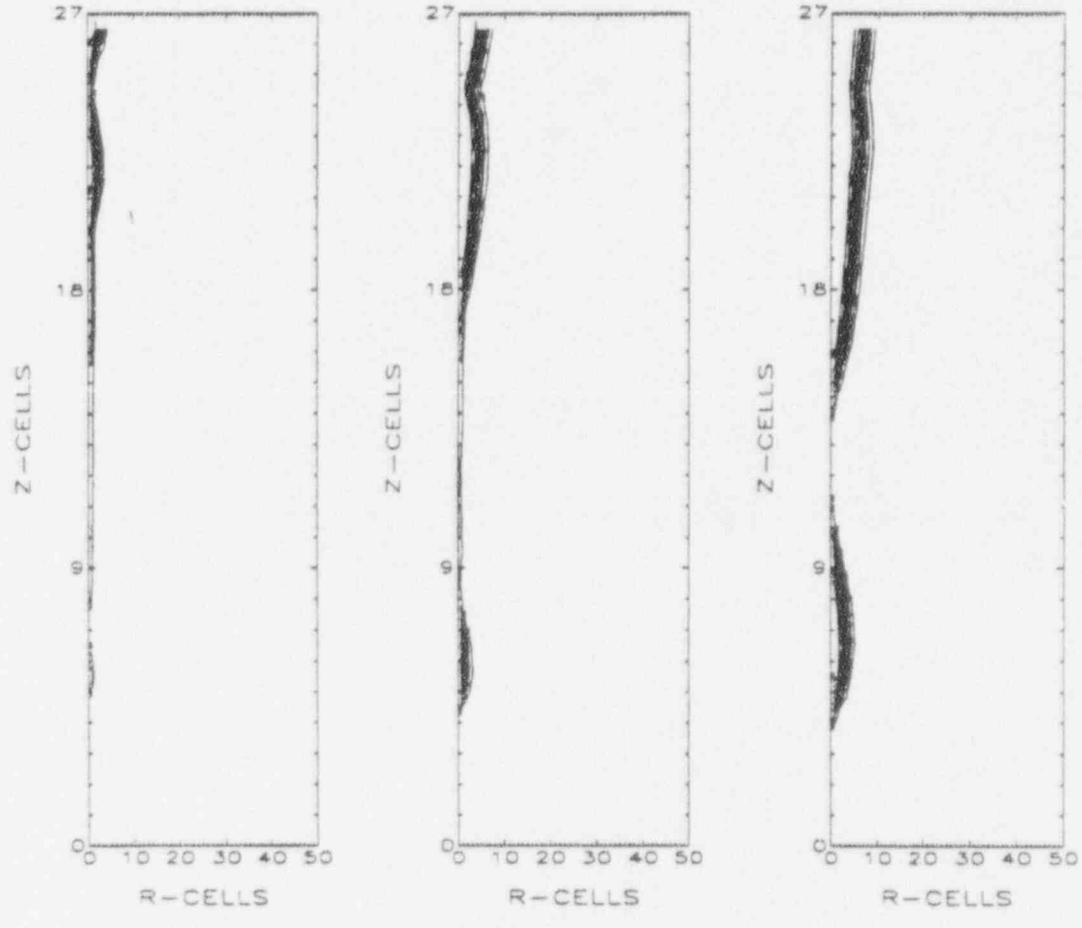

2.5 ms
H=0.9394
L=0.0000

5.0 ms
H=0.9871
L=0.0000

7.5 ms
H=0.9958
L=0.0000

Figure III.6 (contd)
Outer Instrument Tube Failure–Propagation
Void Fraction
(Δr = 3.0 cm, Δz = 20.0 cm)

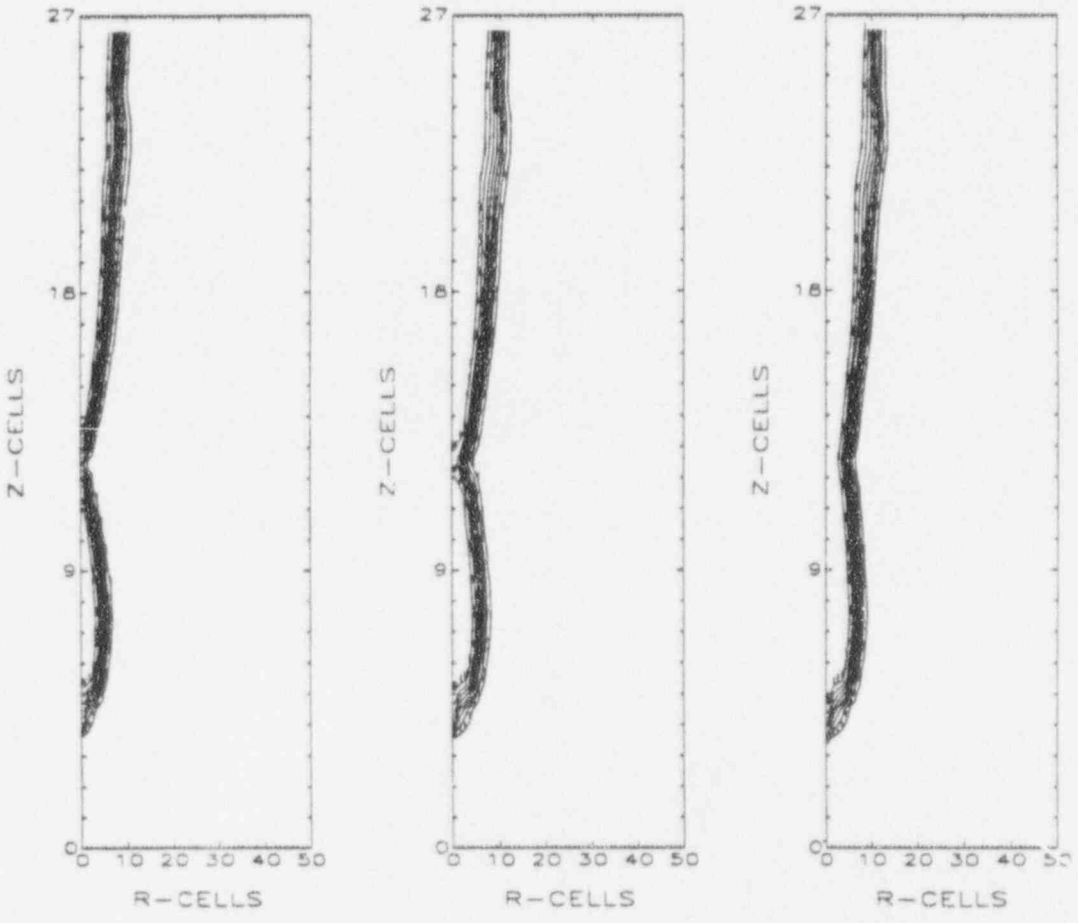

10.0 ms
H=0.9982
L=0.0000

12.5 ms
H=0.9992
L=0.0000

15.0 ms
H=0.9997
L=0.0000

Figure III.7
Outer Instrument Tube Failure–Propagation
Pressure (bar)
(Δr = 3.0 cm, Δz = 20.0 cm)

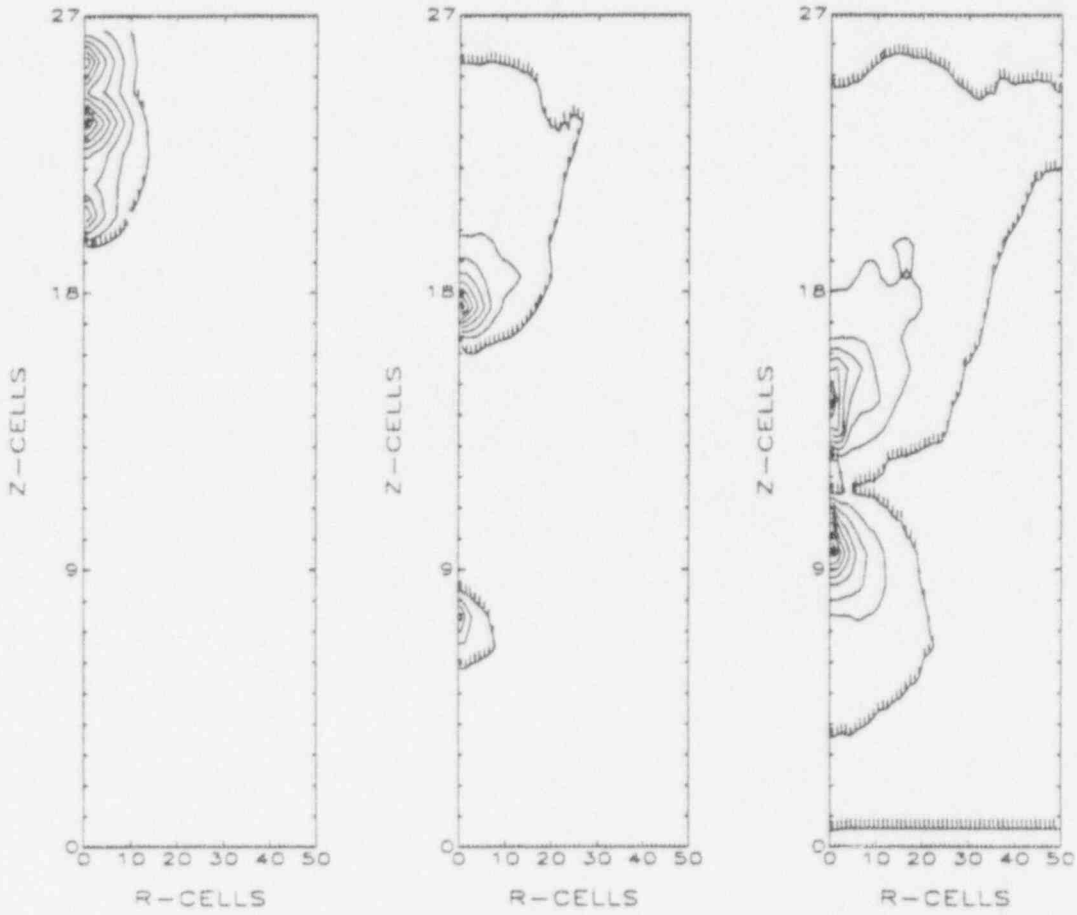

2.5 ms
H=61.26
L=2.061

5.0 ms
H=63.46
L=1.967

7.5 ms
H=38.99
L=1.405

Figure III.7 (contd)
Outer Instrument Tube Failure–Propagation
Pressure (bar)
(Δr = 3.0 cm, Δz = 20.0 cm)

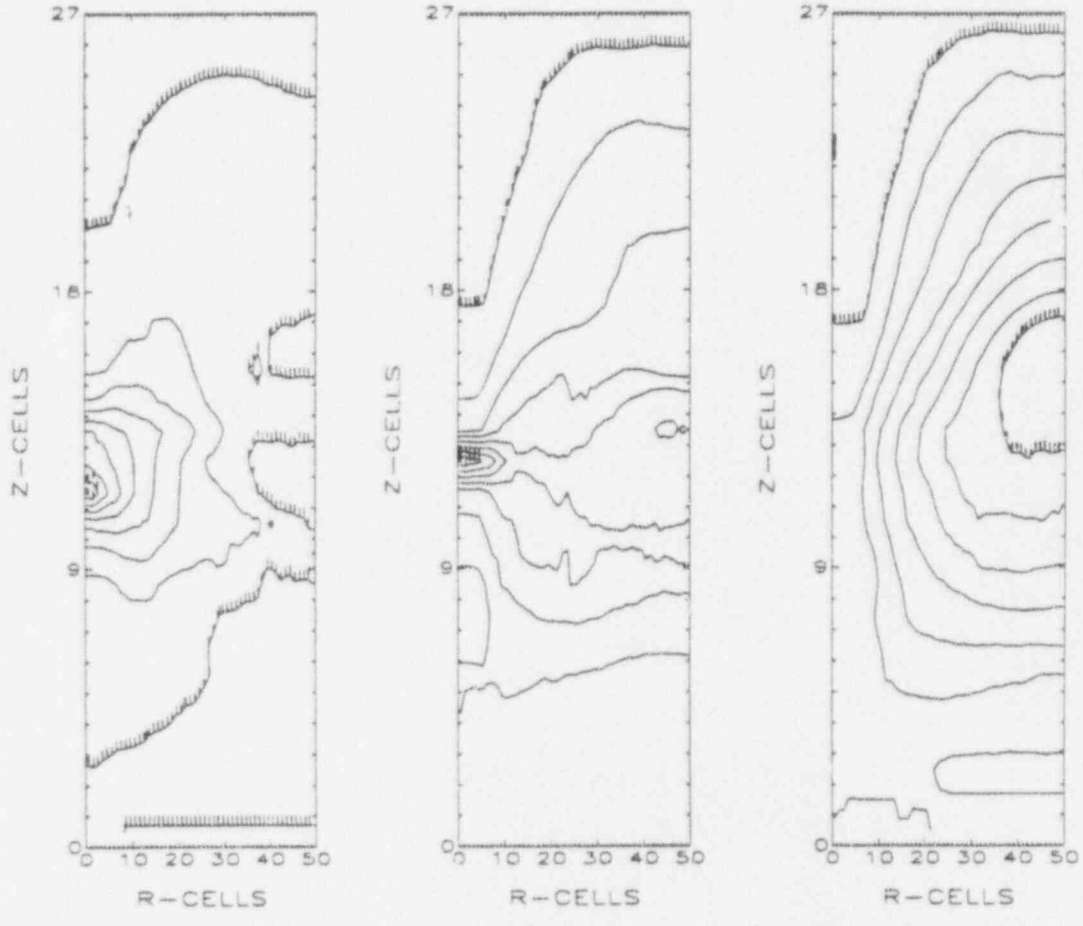

10.0 ms
H=27.99
L=1.636

12.5 ms
H=16.67
L=2.152

15.0 ms
H=12.69
L=2.001

Figure III.8
Outer Instrument Tube Failure–Propagation
Pressure (bar)
(Δr = 3.0 cm, Δz = 20.0 cm)

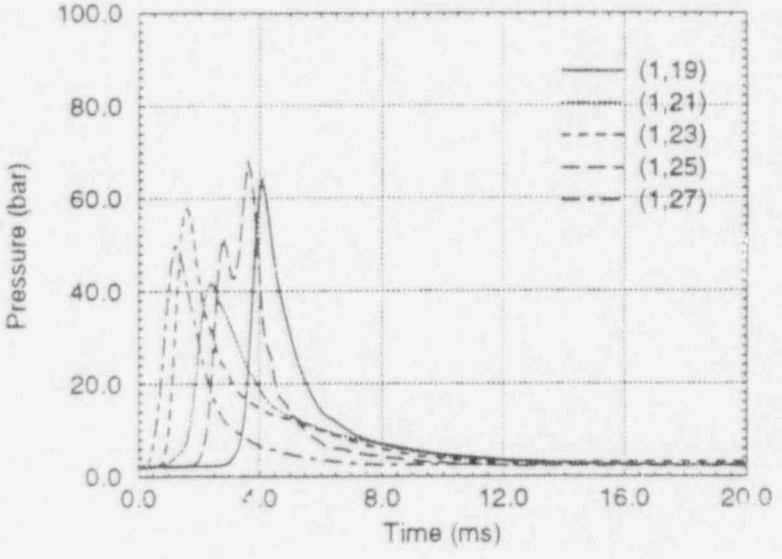

(a) Pressures along melt jet center line

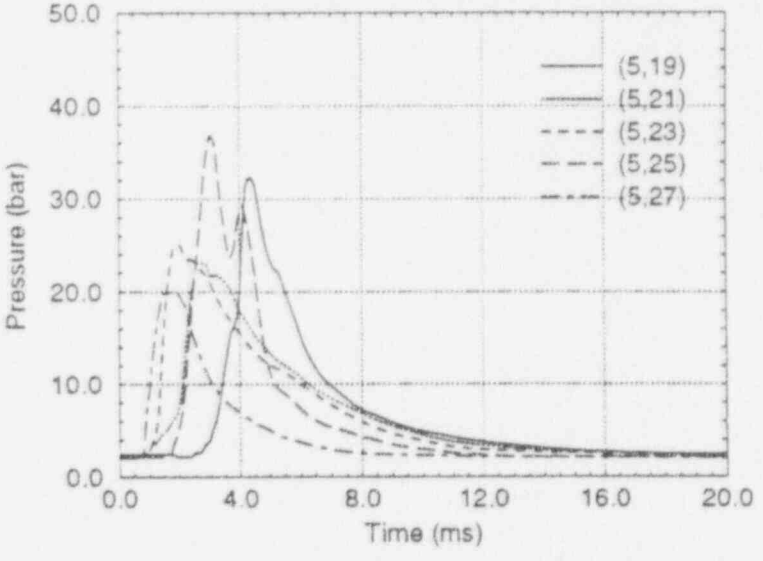

(b) Pressures along corbel support

Figure III.9
Outer Instrument Tube Failure
Impulse ($KPa \cdot s$)
($\Delta r = 3.0$ cm, $\Delta z = 20.0$ cm)

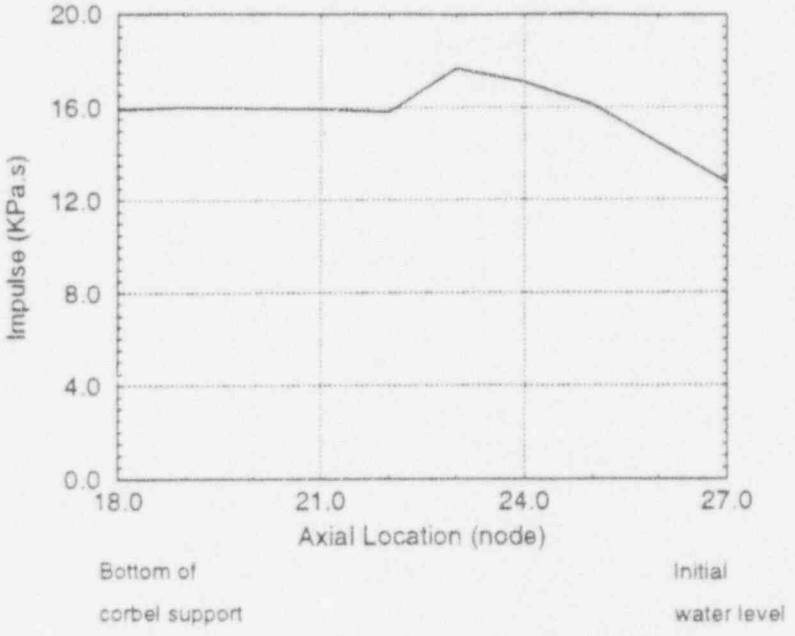

(a) Impulse Distribution Along Center Line

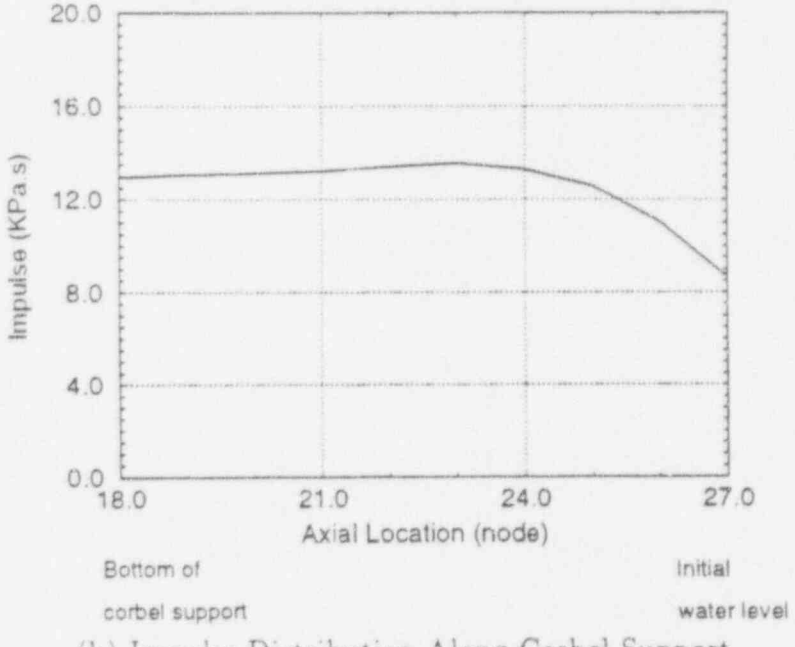

(b) Impulse Distribution Along Corbel Support

RESPONSE TO COMMENTS

I. GENERAL COMMENT

The water pool was assumed to be initially saturated in [1]. We have repeated the calculations for the central instrument rupture and the outer instrument rupture scenarios, using a subcooled water pool temperature of 353 K [2]. In the repeated calculations we have also modified the location of triggering (see response to Comment II.4 below). We did not repeat calculations for the multiple instrument tube rupture, because, as discussed in our report, 2-D calculations for this case do not provide realistic predictions, and 3-D calculations may be required.

II. CENTRAL INSTRUMENT TUBE FAILURE

Comment II.1

The boundary conditions imposed on the top of the computational domain are: a) a constant pressure of 2 bars; and b) a constant, downward velocity for fluid 3, representing the incoming molten fuel jet, and its associated volume fraction, α_3 in the innermost radial node. The boundary conditions in item b provide sufficient information for the specification of the velocity and mass flow rate of the molten fuel. Throughout the simulated transient, furthermore, the top of the computational domain is an open port, through which fluids 1 and 2, representing gas and liquid coolant phases, respectively, are allowed to flow as required by the conservation equations.

Comment II.2

The velocity and the path of the fuel particles in the water pool represent the solutions of the momentum conservation equations. The molten fuel has a significantly higher density than water, and velocity of the fuel particles remains high due to their large inertia. One can, of course, manipulate this by modifying the drag coefficient correlations in the code. This however, would be inappropriate.

During premixing, when there is no significant convective flow in the water pool, the fuel particles are predicted by the code to move straight downward in the water pool, and they undergo significant radial distribution only after they impact the bottom of the pool. This is expected. Heavy particles sinking in quiescent liquids may move zigzag as they sink, nevertheless, their overall path should remain vertical.

Comment II.3

In the referenced figures contours of equal void fractions are shown. The contours indicate that void fraction is very high along the path, and at the immediate vicinity, of the fuel jet, and remains very small far away from the fuel jet.The code's predictions are reasonable.

By "cell-like" structures the reviewers may be referring to the contours in some of the figures, e.g. Figures 2.4 and 3.4 of [1], in which some of the contours are closed curves. During premixing and propagation in saturated water, near-complete local evaporation results in the establishment of a two-dimensional flow field, leading to

the curvature of some of the constant void fraction contours due to lateral motion of the fluid. Note also that the sum of the volume fractions of all fluids at each node should be equal to one, therefore the vapor void fraction in this case has to decrease near the fuel jet centerline due to the presence of fuel.

The enclosed new calculation results obtained with an initially subcooled water pool [2], as noted, generally indicate lower void fractions than the results with an initially saturated water pool, and do not include such "cell-like" structures.

Comment II.4

In the repeated calculations for the central instrument and outer instrument tube rupture scenarios (see response to General Comment I) we have assumed that triggering takes place in node (1,23) 4.5 m above the pool bottom. This location correctly represents the midplane of the submerged portion of the corbel support structure.

Regarding the effect of the triggering strength on the predicted results, please see Section II.3 of the enclosed supplement report [2], where we have compared results obtained assuming 10% and 20% fuel fragmentation in one time step (2 μs), in the triggered node. These results, as noted, indicate that the pressure histories far away from the triggering location are relatively insensitive to the triggering strength. They also indicate that the impulse distribution in the explosion zone is only slightly affected.

The assumed size and strength of the trigger are arbitrary, nevertheless. The im-

position of a strong local fragmentation is a reasonable way of simulating spontaneous triggering in computations. Sensitivity studies are needed to examine the effect of both the strength and location of the triggering event.

Comment II.5

In the repeated calculations for central instrument tube and outer instrument tube failure scenarios discussed in the enclosed supplement report [2] (see also response to General Comment I) we have included the calculated pressure impulse distributions for both the molten fuel jet centerline and the corbel support surface. The calculated results for both the initially saturated and subcooled water pool cases are once again lower than those predicted by the TEXAS code.

Comment II.6

This is a matter of degree. We agree with the comment that a 10-20% difference in the calculated results is well within the uncertainties of such calculations.

Comment II.7

The new calculation results representing an initially subcooled water pool, depicted in Figure II.7 of the enclosed supplement report [2] give somewhat different numbers. The maximum depicted pressure at corbel support (node (50,19) in Figure II.7 b) is approximately 6.5 bars, compared with a maximum pressure of approximately 26 bars at the same elevation on the centerline (node (1,19) in Figure II.7a).

One should remember that the explosion zone is approximately a cylinder. Follow-

ing triggering, the code predicts multiple explosions at various heights. The apparent flat pressure histories at the corbel support surface are due to the arrival of pressure waves, resulting from these multiple explosions, at different times. The arriving pressure waves tend to overlap and hence it is not a straightforward matter to attenuate the calculated pressure histories from 1-D calculations to the outer boundaries of the calculated domain. We agree that the calculated impulse on the corbel support would be somewhat higher, had the calculation been performed for a longer period. However, as can be seen in Figure II.7 and III.8, the calculated impulse values along the molten fuel jet centerline are reasonable since, within 20 ms after triggering (which represents the integration time period for calculated impulses), the pressures have decreased to the base pressure value.

III. OUTER INSTRUMENT TUBE FAILURE

Comment III.1

Please see responses to comments II.1, II.2, and II.3.

Comment III.2

We agree with the reviewers' comment regarding the conservative nature of pressure histories predicted by using a 30 cm-diameter cylindrical computational zone.

In the enclosed supplement report [2] we have repeated the simulation of outer instrument rupture scenario where we have used a computational domain 300 cm in diameter (Figure III.4 in the supplement report), as suggested by the reviewers.

The computational domain is entirely fluid, however, and does not include any flow obstruction. In these calculations, furthermore, the initial pool temperature was assumed to be 353 K, and triggering was simulated 4.5 m above the pool bottom. The predicted pressure histories for the molten fuel jet centerline and the radial nodes representing the physical location of the corbel support surface are shown in Figures III.8a and III.8b of the supplement report [2]. Comparing these figures with the results representing the central tube failure case (Figures II.7 a and II.7 b in the supplement report [2]), it can be noted that the predicted peak pressures in the two cases are comparable, and the differences can be attributed at least partially to the differences between the two systems at the end of premixing (the molten fuel jet has a slightly lower velocity in the outer instrument tube failure scenario). The predicted pressures along the corbel support surface, as expected, are significantly higher for the outer instrument tube failure, due to the proximity to the explosion zone.

It should be noted that placing a flow obstruction in a large computational domain in order to simulate the geometry of this system will make the problem three dimensional. Simulation of the problem using a 2-D (r,z) coordinate system, as suggested by the reviewers, is not possible. Rigorous and realistic simulation of this scenario will need a 3-D analysis.

IV. MULTIPLE INSTRUMENT TUBE FAILURE

Comment IV.1

We agree that the calculated results for this case were unrealistic, as stated in our report [1]. Furthermore, as we mentioned in [1], we believe that this scenario needs a 3-D calculation.

Comment IV.2

The calculations were presented in order to demonstrate the inadequacy of coarse nodalization, and convey the conclusion that this problem requires a 3-D simulation.

V. RECOMMENDATIONS FOR FUTURE WORK

Comment V.1

Calculations where the effect of the location of triggering is parametrically varied are recommended because the location of triggering may affect the pressure histories and pressure impulses.

In the absence of an external trigger, triggering due to the impact of the molten material on solid surfaces is a well-recognized and experimentally-observed phenomenon. This type of triggering is likely to happen in the real systems.

Parametric examination of the effect of the location of triggering should of course be done using a realistic simulation of the propagation phase. We therefore agree with the reviewers that such parametric calculations using the small 30 cm-diameter cylindrical computational domain will not be adequate. These parametric calculation,

however, can be done with the large computational domain used in the supplement report [2], and should certainly be done with a 3-D simulation, should such simulation be deemed necessary.

Comment V.2

Realistic quantification of the consequences of the failure of multiple instrument tube penetrations needs a 3-D simulation. A 2-D simulation, even with very small radial nodes, will not be quite adequate since replacing circular jets with annuli is inappropriate.

Performing a 3-D calculation with a small segment of the system, say 1/4 of the circular cross-section of a large computational zone which includes blocked flow areas, can be a reasonable compromise for addressing multi-dimensionality and maintaining the computational cost under control. The nonuniformity of the distribution of tube penetration locations can be dealt with by approximating the geometry with an equivalent symmetric distribution. Such an approximation would be far more realistic than replacing the jets with circular annuli. Furthermore, by performing two parametric calculations, representing upper and lower bounds for the concentration of the penetrations in the assumed symmetric geometry, one can bracket the exact solution results within a rather small bound.

Regarding adequate experimental validation of parametric fine fragmentation model in $GT3F^{TM}$, lack of sufficient validation applies to all the results and is not limited

to the multi-penetration case. It also applies to all existing steam explosion models.

VI. PARTICLE BREAKUP AND FINE FRAGMENTATION MODELS IN $GT3F^{TM}$ COMPUTER CODE

Comment VI.1

Both typographical errors have been corrected.

Comment VI.2

The method for calculating the molten fuel surface area in $GT3F^{TM}$ will be explained in the following paragraph. However, the reviewers should be reminded that the intention of providing Appendix A, as clearly stated in Reference [1], was to describe details of the breakup model only. Further modeling details, relevant to the issue raised in this comment or otherwise, should be obtained from References [3,4] (References [2,3] in the supplement report [2]).

The total surface area of the fuel is calculated from:

$$a_{13} + a_{23} = \frac{6\alpha_3}{D_3} \tag{1}$$

where a_{13} and a_{23} are specific surface areas (surface areas per unit mixture volume) between fluids 1 and 3, and between fluids 2 and 3, respectively, and α_3 is the volume fraction of the molten fuel in the mixture. Thus, the total surface area of the molten material is calculated by assigning an average, hydrodynamically-controlled diameter to the fuel particles. Now, the way this specific area is distributed among a_{13} and

a_{23} depends on which one of the two fluids 1 (gas) and 2 (liquid) is continuous. The reviewers should consult References [3,4] (References [2,3] of the supplement report) for further details.

Comment VI.3

The specification of 1 cm as the lower bound on fuel particle diameter only applies to the premixing calculations, and is based on comparison of model-predicted pressure peaks during the subsequent propagation phase with KROTOS-21 test results.

Equation 19 in [1] represents the $GT3F^{TM}$ hydrodynamic breakup model for: a) the premixing phase, as long as the fuel particles are larger in diameter than 1 cm; and b) for the propagation phase, without any bound.

Comment VI.4

Freezing of the melt particles is included in the simulation. Frozen particles are not allowed to undergo fine fragmentation.

In Equation (18) of [1] the critical Weber number is the only adjustable parameter.

$GT3F^{TM}$ does not consider thermal effects in its modeling of fine fragmentation.

VII. SIMULATION OF KROTOS-21 STEAM EXPLOSION EXPERIMENT

Comment VII.1

KROTOS-21 was a 1-D test, and was therefore simulated using a 1-D nodalization. Radial nodalization is thus irrelevant.

Comment VII.2

We agree with the reviewers on their point that the fragmentation model in $GT3F^{TM}$ needs further validation. We plan to perform more validation calculations, in which we will include more KROTOS tests.

REFERENCE

1. *Analysis of Ex-vessel Steam Explosions for the Combustion Engineering System 80+ using the $GT3F^{TM}$ Computer Code*, Attachment to letter from S. I. Abdel-Khalik and S. M. Ghiaasiaan to M. Khatib-Rahbar (June 3, 1994).

2. H. Esmaili and M. Khatib-Rahbar, *Analysis of Ex-vessel Steam Explosions for the Combustion Engineering System 80+*, ERI/NRC 94-201, Energy Research, Inc. March 1994.

3. W. M. Ren, S. M. Ghiaasiaan, and S. I. Abdel-Khalik, *GT3F: An Implicit Finite-Difference Computer Code for Transient Three-Dimensional Three-Phase Flow Part I: Governing Equations and Solution Scheme*, Numerical Heat Transfer, Part B: Fundamental, Vol. 25, pp. 1-20, 1994.

4. W. M. Ren, S. M. Ghiaasiaan, and S. I. Abdel-Khalik, *GT3F: An Implicit Finite-Difference Computer Code for Transient Three-Dimensional Three-Phase Flow Part II: Applications*, Numerical Heat Transfer, Part B: Fundamental, Vol. 25, pp. 21-38, 1994.

Figure II.9
Central Instrument Tube Failure–Propagation
Pressure (bar)
($\Delta r = 3.0$ cm, $\Delta z = 20.0$ cm, 20% Triggering)

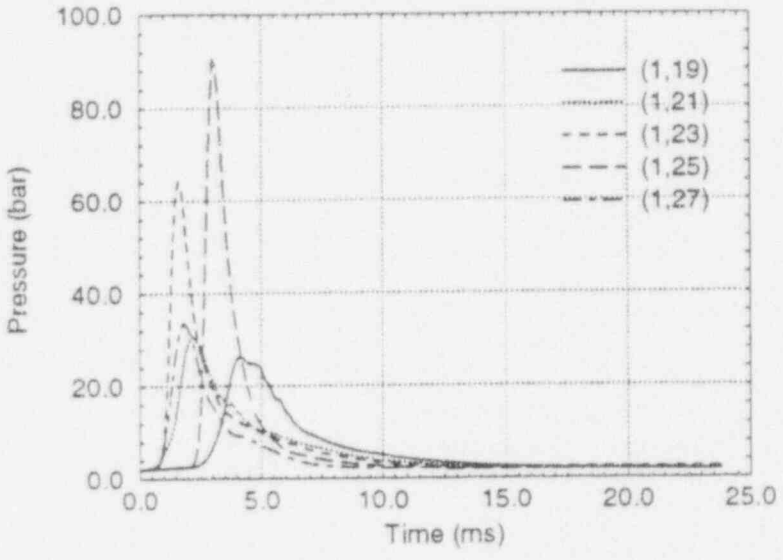

(a) Pressures along melt jet center line

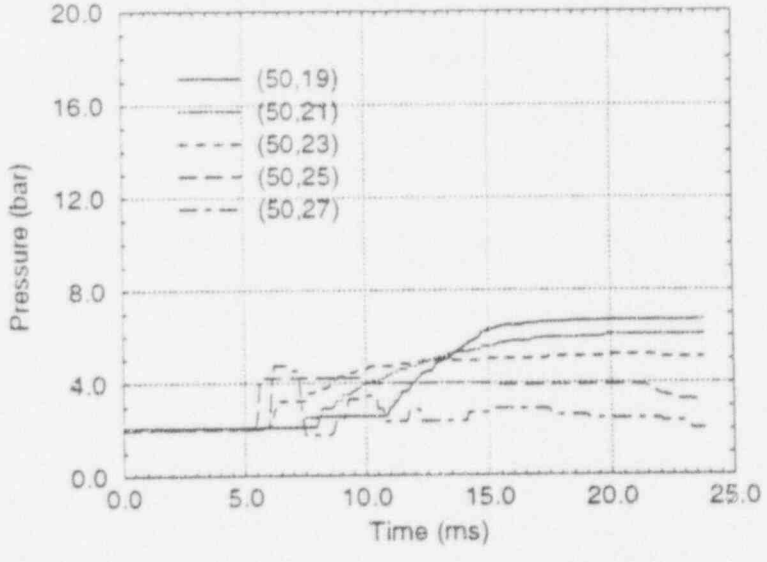

(b) Pressures along corbel support

Figure III.1 (Corresponding to Figure 3.3 in [1])
Outer Instrument Tube Failure–Premixing
Fuel Volume Fraction
($\Delta r = 3.0$ cm, $\Delta z = 20.0$ cm)

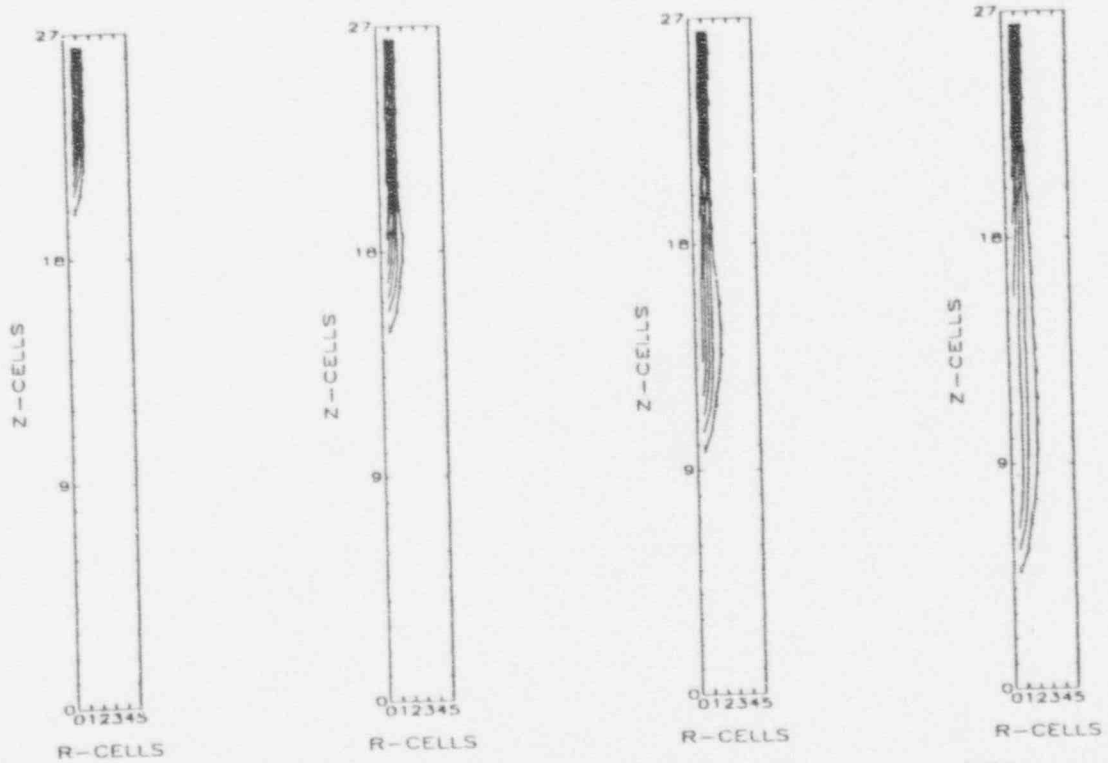

0.25 sec
H=0.2333
L=0.0000

0.50 sec
H=0.2422
L=0.0000

0.75 sec
H=0.2447
L=0.0000

1.00 sec
H=0.2425
L=0.0000

Figure III.2 (Corresponding to Figure 3.4 in [1])
Outer Instrument Tube Failure–Premixing
Void Fraction
($\Delta r = 3.0$ cm, $\Delta z = 20.0$ cm)

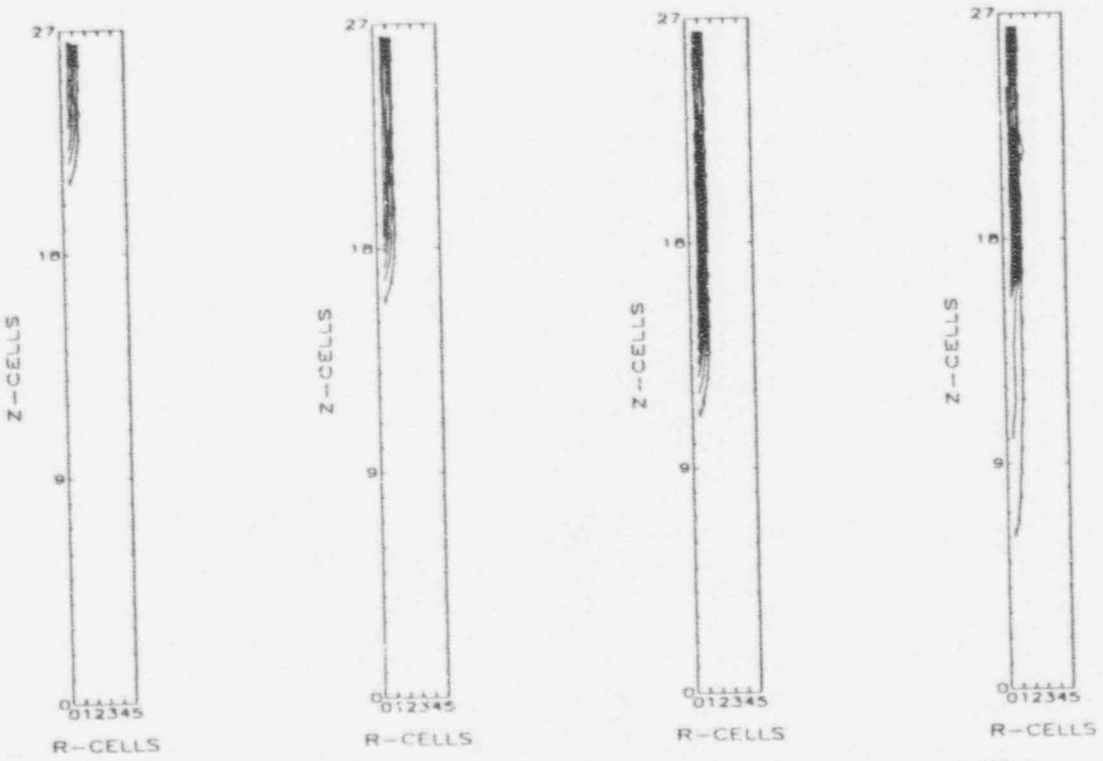

0.25 sec
H=0.6894
L=0.0001

0.50 sec
H=0.5993
L=0.0001

0.75 sec
H=0.7001
L=0.0001

1.00 sec
H=0.6549
L=0.0001

Figure III.3 (Corresponding to Figure 3.5 in [1])
Outer Instrument Tube Failure–Premixing
Pressure (bar)
($\Delta r = 5.0$ cm, $\Delta z = 20.0$ cm)

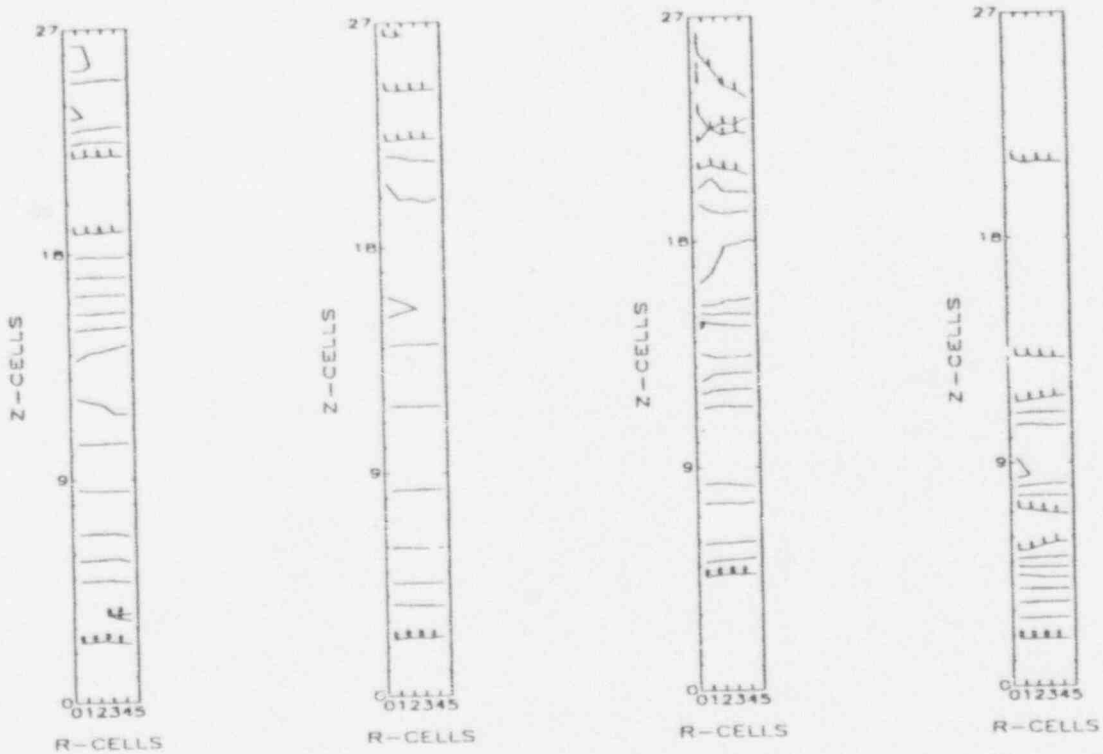

0.25 sec
H=2.381
L=1.878

0.50 sec
H=2.828
L=1.921

0.75 sec
H=2.290
L=1.971

1.00 sec
H=4.601
L=2.014

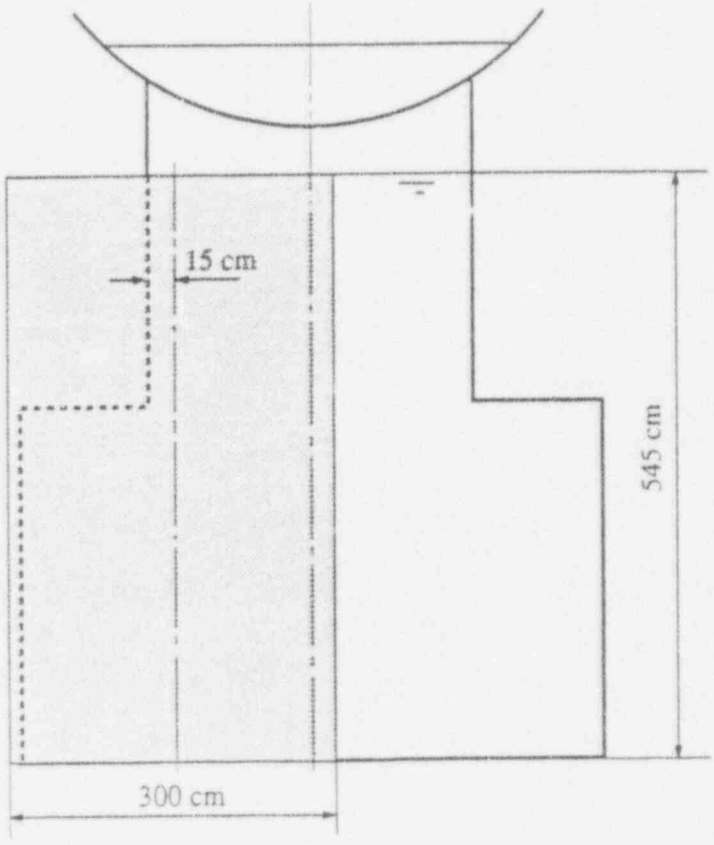

Figure III.4: Outer Instrument Tube Failure
(Shaded area represents computational domain for propagation calculation)

Figure III.5
Outer Instrument Tube Failure–Propagation
Fuel Volume Fraction
(Δr = 3.0 cm, Δz = 20.0 cm)

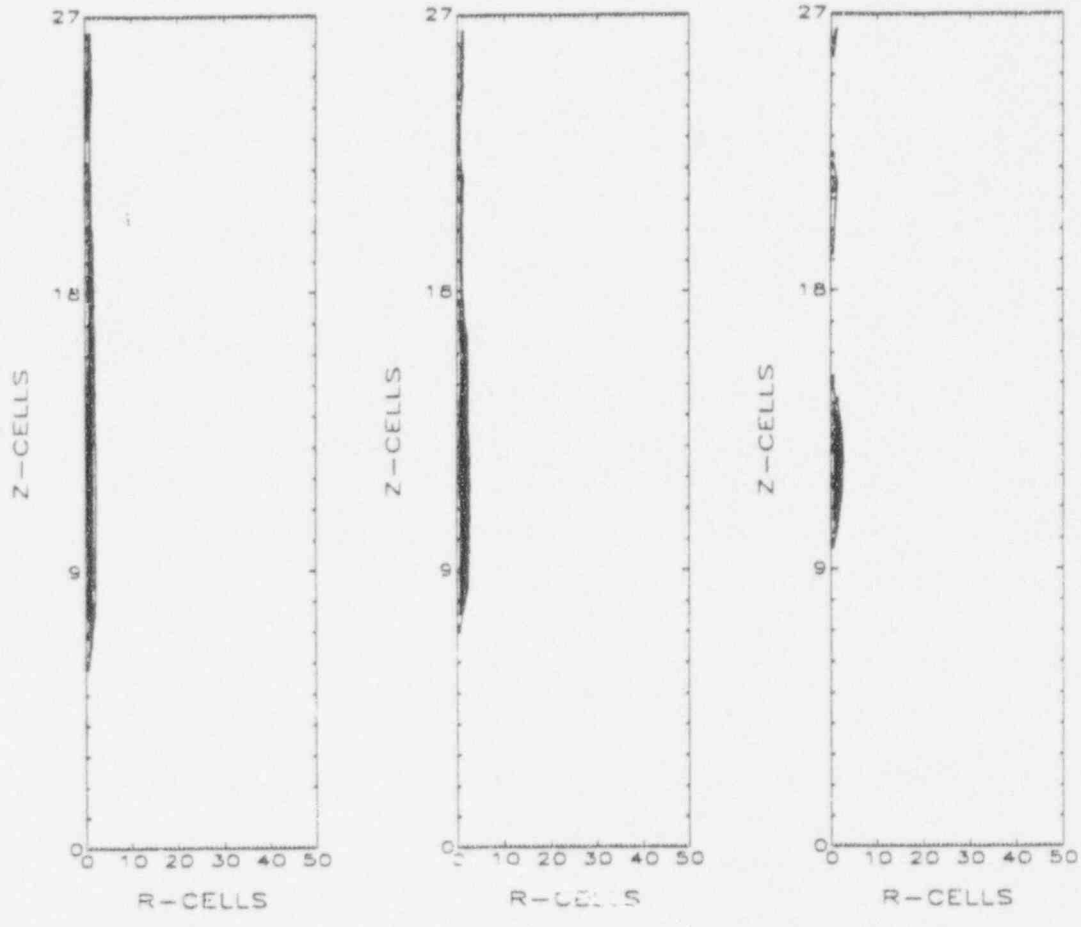

2.5 ms
H=0.2247
L=0.0001

5.0 ms
H=0.1080
L=0.0001

7.5 ms
H=0.1015
L=0.0001

Figure III.5 (contd)
Outer Instrument Tube Failure–Propagation
Fuel Volume Fraction
(Δr = 3.0 cm, Δz = 20.0 cm)

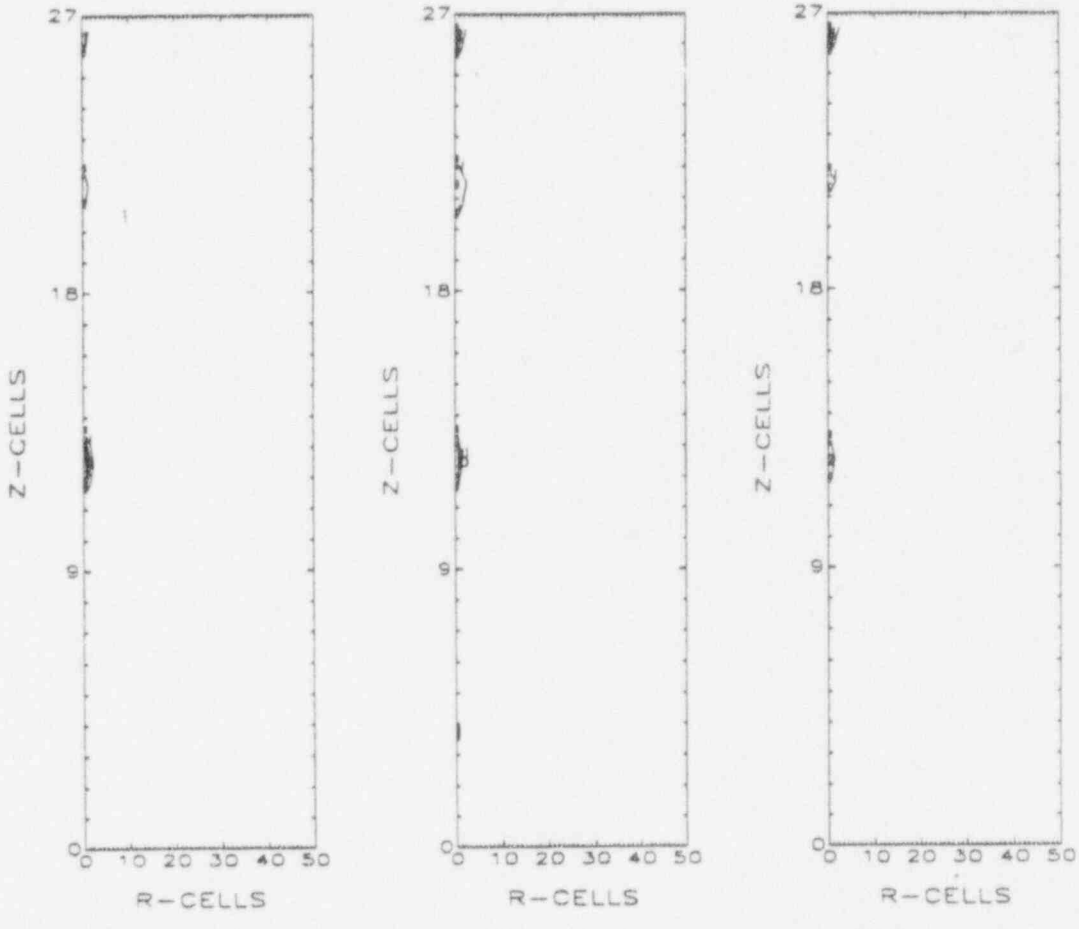

10.0 ms
H=0.0951
L=0.0001

12.5 ms
H=0.0419
L=0.0001

15.0 ms
H=0.0469
L=0.0001

Figure III.6
Outer Instrument Tube Failure–Propagation
Void Fraction
(Δr = 3.0 cm, Δz = 20.0 cm)

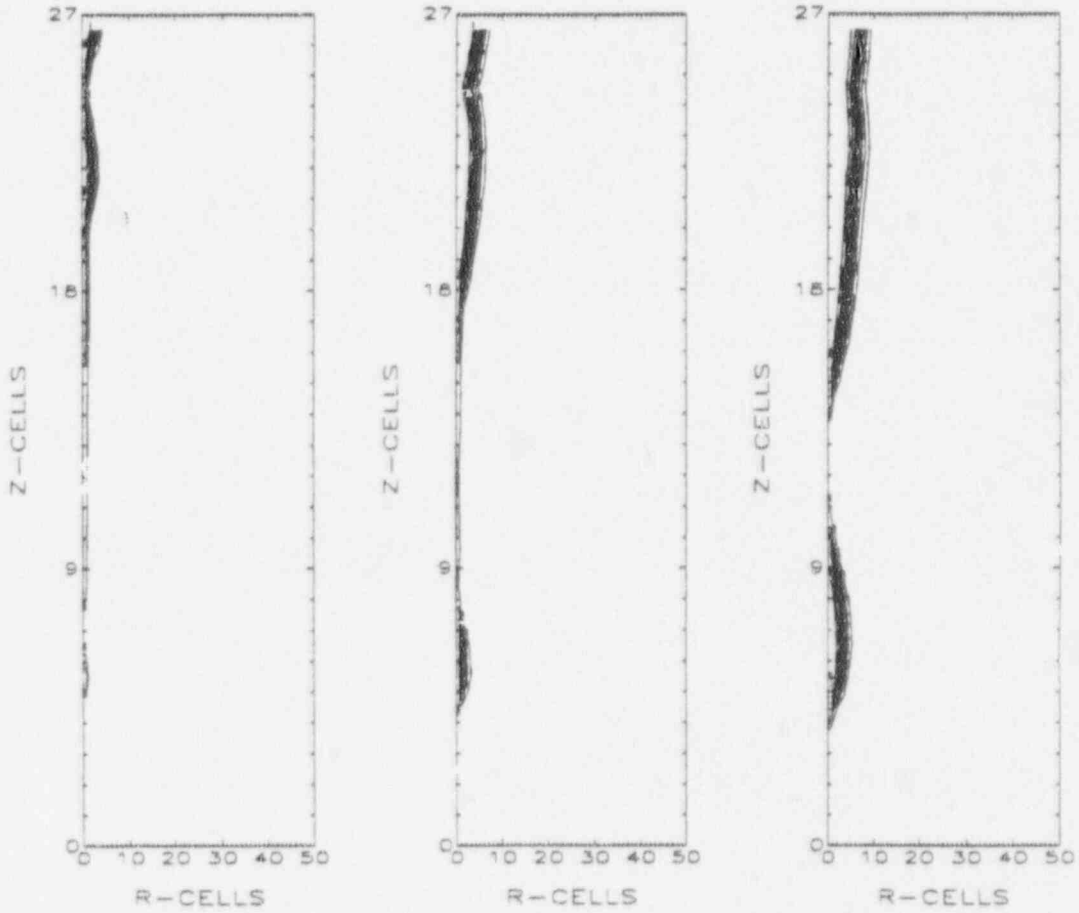

2.5 ms
H=0.9394
L=0.0000

5.0 ms
H=0.9871
L=0.0000

7.5 ms
H=0.9958
L=0.0000

Figure III.6 (contd)
Outer Instrument Tube Failure–Propagation
Void Fraction
($\Delta r = 3.0$ cm, $\Delta z = 20.0$ cm)

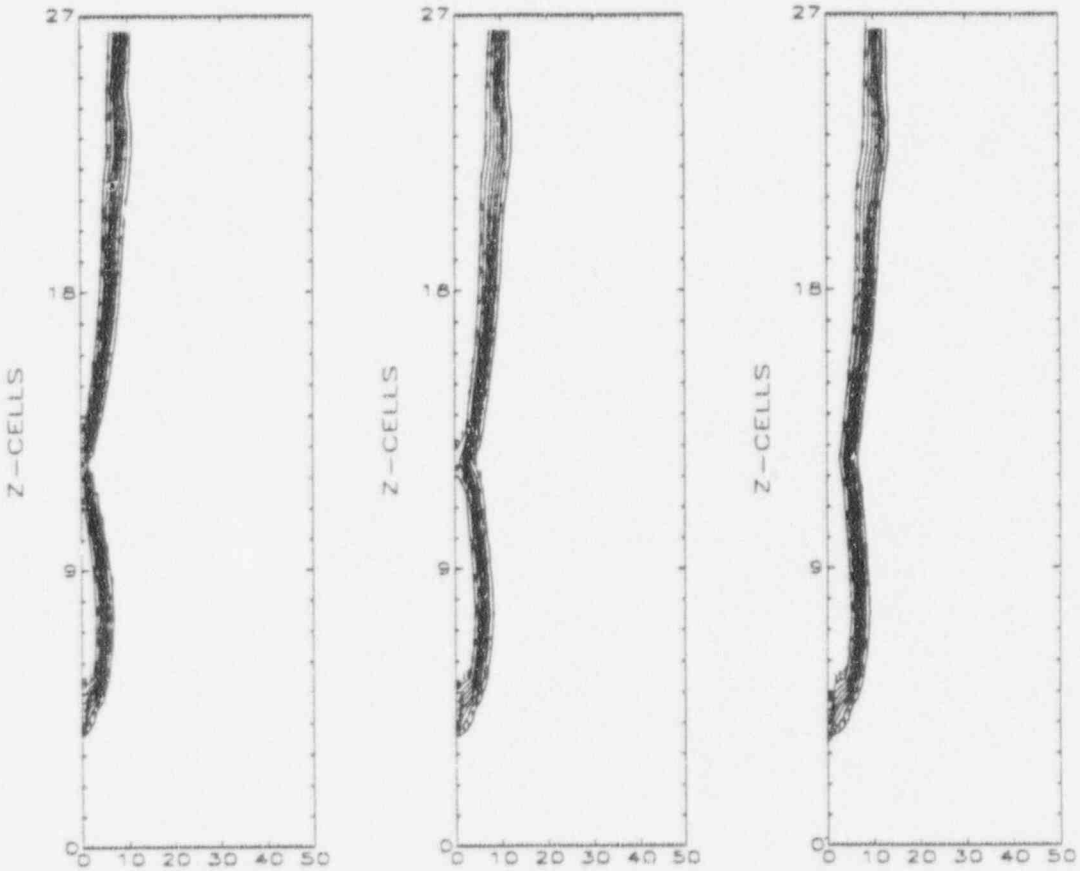

Figure III.7
Outer Instrument Tube Failure–Propagation
Pressure (bar)
(Δr = 3.0 cm, Δz = 20.0 cm)

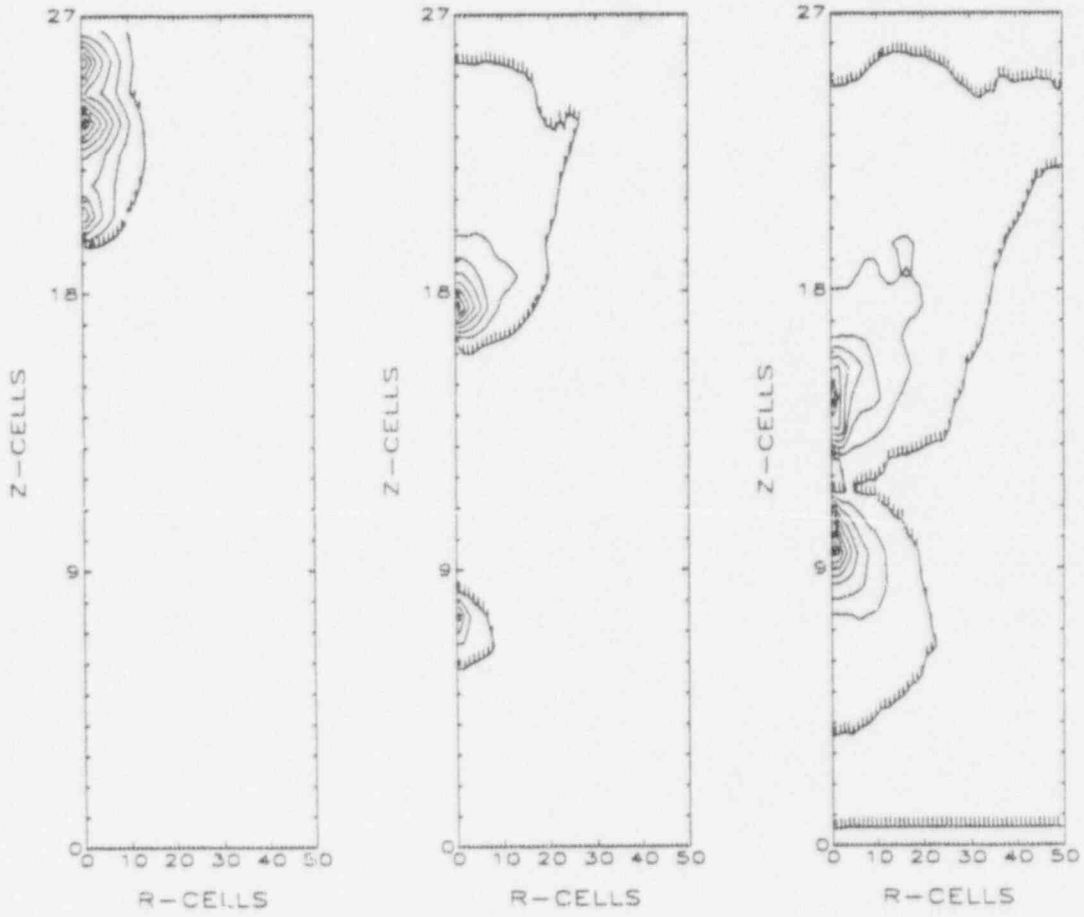

2.5 ms
H=61.26
L=2.061

5.0 ms
H=63.46
L=1.967

7.5 ms
H=38.99
L=1.405

Figure III.7 (contd)
Outer Instrument Tube Failure–Propagation
Pressure (bar)
(Δr = 3.0 cm, Δz = 20.0 cm)

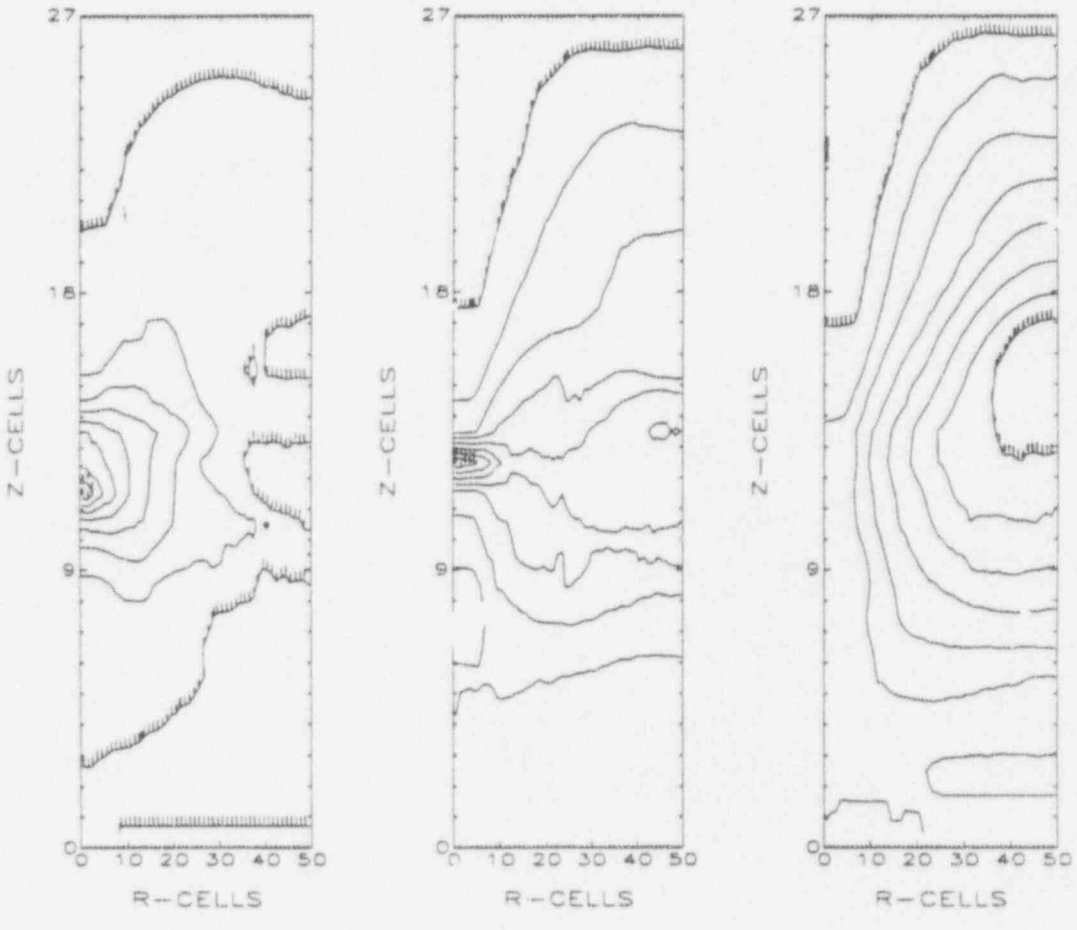

10.0 ms
H=27.99
L=1.636

12.5 ms
H=16.67
L=2.152

15.0 ms
H=12.69
L=2.001

Figure III.8
Outer Instrument Tube Failure–Propagation
Pressure (bar)
(Δr = 3.0 cm, Δz = 20.0 cm)

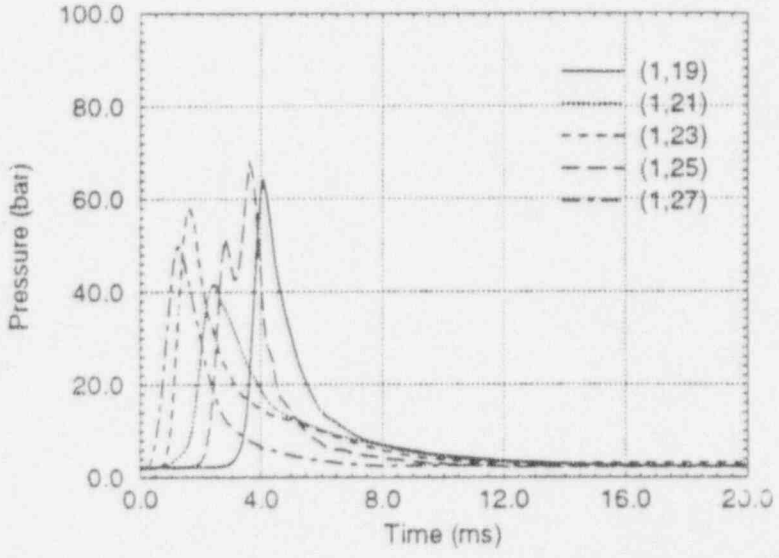

(a) Pressures along melt jet center line

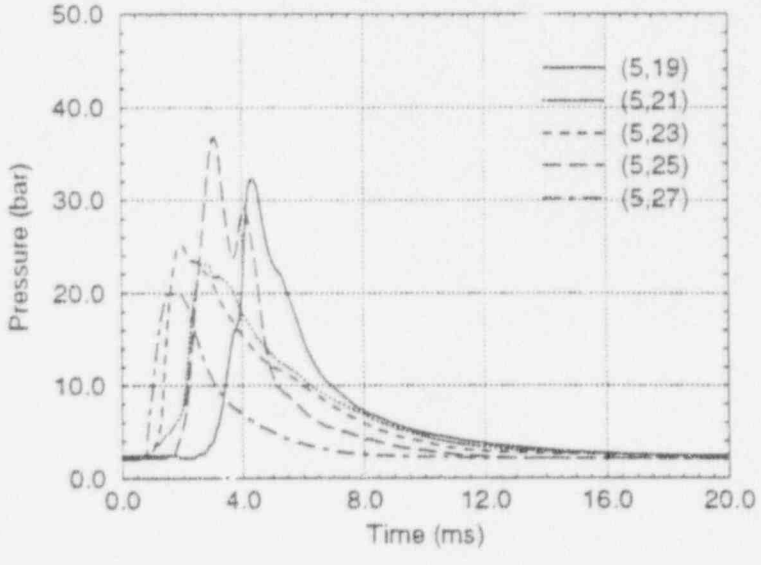

(b) Pressures along corbel support

Figure III.9
Outer Instrument Tube Failure
Impulse ($KPa \cdot s$)
($\Delta r = 3.0$ cm, $\Delta z = 20.0$ cm)

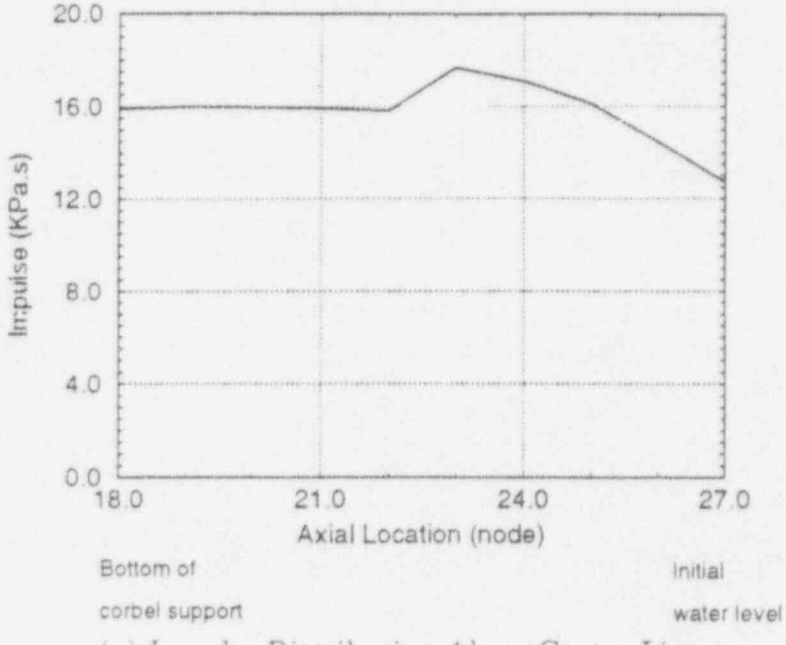

(a) Impulse Distribution Along Center Line

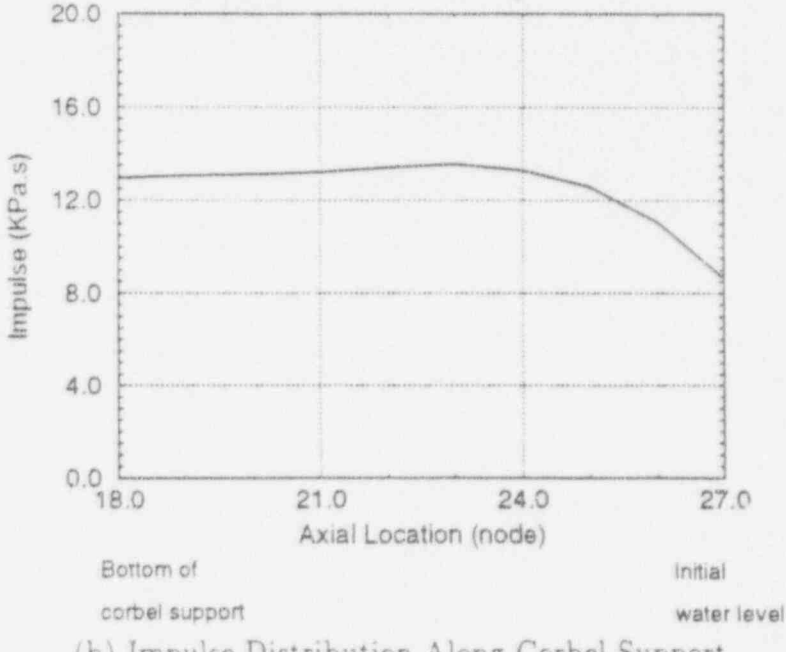

(b) Impulse Distribution Along Corbel Support